Bachelor's Thesis

Design, Simulation, and Evaluation of a Load Balancing Algorithm for Peer-to-Peer-Networks based on Push-Pull Sum and Deal-Agreement-Based Algorithms

Emre Bayazıtoğlu

Examiner: Prof. Dr. Christian Schindelhauer
Advisers: Saptadi Nugroho

University of Freiburg

Faculty of Engineering

Department of Computer Science

Chair of Computer Networks and Telematics

February 25th, 2025

Writing Period

18. 12. 2024 – 18. 03. 2025

Examiner

Prof. Dr. Christian Schindelhauer

Advisers

Saptadi Nugroho

Declaration

I hereby declare that I am the sole author and composer of my thesis and that no other sources or learning aids, other than those listed, have been used. Furthermore, I declare that I have acknowledged the work of others by providing detailed references of said work.
I hereby also declare that my Thesis has not been prepared for another examination or assignment, either wholly or excerpts thereof.

Place, Date	Signature

Abstract

The Push-Pull Sum algorithm, introduced in [1], combines elements of the Push-Sum [2] and Pull-Sum algorithms. The Push-Sum algorithm, proposed by Kempe et al., is a load balancing method where each node randomly selects a neighbor and transfers half of its current sum and weight to that neighbor. Load balancing algorithms are designed to evenly distribute loads across networks, typically modeled as undirected graphs. In such networks, nodes exchange loads with their neighbors to achieve a balanced state. The Single-Proposal Deal-Agreement-Based load balancing algorithm, as presented in [3], incorporates a deal-agreement mechanism into load transfers in order to achieve fair load transfers between two nodes.

In this thesis, I propose and implement a variation of the Push-Pull Sum algorithm that integrates principles from the Deal-Agreement-Based algorithm and adaptive thresholding. This adaptation modifies and extends certain properties of the original Push-Pull Sum algorithm. For the Adaptive Threshold Push-Pull Sum algorithm, I provide pseudocode, implement the different load balancing approaches in a peer-to-peer network, and analyze simulation outcomes across different topologies. The objective is to find a compromise solution including overall good performance in different topologies. The performance of this algorithm is evaluated using the mean squared error (MSE) reduction over time as a convergence metric. Results are presented using log-log and log-linear graphs to compare the efficiency of error reduction in various scenarios. The slopes of the MSE curves give insights into how effectively the algorithms distribute loads across the network. Additionally, the data

is fitted to different models to assess the rate of convergence per region.

The findings suggest that the proposed modifications to the Push-Pull Sum algorithm achieve a more efficient and scalable load balancing strategy for most of the scenarios tested in the experiments. The adaptive threshold mechanism added to the Push-Pull Sum algorithm dynamically adjusts the threshold based on the state of imbalance in the network, making it efficient in dense graphs as well as low regular degree graphs. In some of the topologies under test, the Adaptive Threshold Push-Pull Sum algorithm acts as an intermediate solution between the Deal-Agreement-Based and Push-Pull Sum algorithms.

Contents

List of Figures

List of Tables

List of Algorithms

Listings

1 Introduction

In times where computational tasks are becoming increasingly heavy, many systems require multiple servers or computers to complete these tasks. These servers, or computers, often referred to as nodes, interact directly with each other, are decentralized, and form a so-called peer-to-peer network. As depicted in figure 1, each node consists of a CPU, a memory module, and a network interface for communication with other nodes. Together, these nodes form a scalable network. The memory system is modeled as a distributed memory scheme, where each node has its own memory module, rather than a shared one, in order to avoid bottlenecks in memory access [4].

Each computer is assigned a non-negative workload, referred to as load, which can represent various computational tasks such as CPU usage, memory utilization, or internet traffic. The main objective when applying load balancing algorithms is to balance the state of the network, meaning that each node holds the average load of the network. This is accomplished by addressing overloading and underloading through the redistribution of load to other nodes. Heavily overloaded nodes risk failing to complete their tasks due to overheating. Therefore, load balancing not only enhances coordination in distributed systems but also improves scalability and ensures high availability.

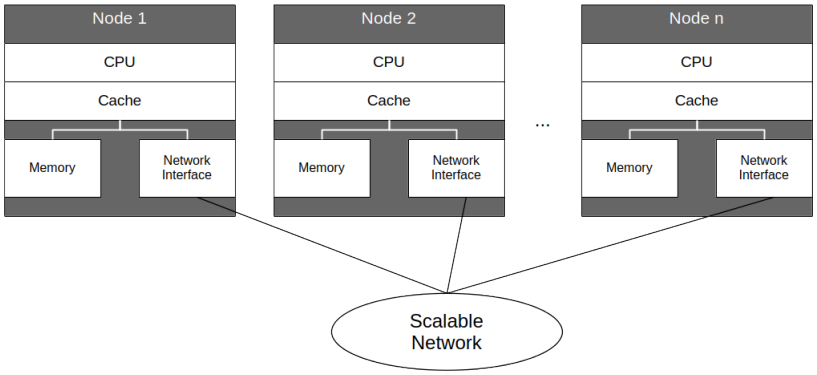

Figure 1: Overview of the setting

1.1 Preliminaries

A graph G is defined as $G = (V, E \subseteq V \times V)$, where $V := \{v_0, v_1, ..., v_{n-1}\}$ represents the vertices (or nodes) of G and $E := \{e_1, e_2, ..., e_{n-1}\}$ represents the edges. The graph may consist of a single vertex and no edges. The number of vertices $|V|$ is often referred to as the order of G. A vertex and an edge are incident if the vertex is an endpoint of the edge. The degree of a vertex is the number of incident edges. If an edge connects two vertices, these vertices are adjacent to each other, thus are neighboring vertices. A loop is an edge that connects a vertex to itself. Multiple edges refer to edges that share the same pair of endpoints. A simple graph has no loops or multiple edges. A clique is a set of pairwise adjacent vertices. A path is a simple graph whose vertices can be ordered such that two vertices are adjacent if and only if they are consecutive in the list. A graph is connected if each pair of vertices in the graph belongs to a path. Bipartite graphs are graphs where the set of graph edges is the union of two disjoint independent sets. If G has a path from node u to node v, then the distance from u to v, $d_G(u, v)$, is the shortest length from a u, v-path. The diameter of the graph $\text{diam}(G) := max_{u,v \in V} d_G(u, v)$ is the greatest length of any of the shortest paths between any two nodes. [5]

1.2 Motivation

The motivation for this thesis stems from the observed performance discrepancies between the Single-Proposal Deal-Agreement-Based algorithm proposed by Yefim Dinitz, Shlomi Dolev, and Manish Kumar [3] and the Push-Pull Sum algorithm described in the paper by Saptadi Nugroho, Alexander Weinmann, and Christian Schindelhauer [1] across different network topologies. These observations were initially gathered during the student project titled "Comparative Analysis of Load Balancing Algorithms in General Graphs" [6]. According to the simulations conducted in the student project, the Push-Pull Sum algorithm performs better in reducing the MSE per round for the Complete graph and the Star graph compared to the Deal-Agreement-Based algorithm, which performs better in reducing the MSE per round for the Torus Grid graph and the Ring graph. The simulations were conducted for different network sizes. The simulations were conducted across networks of varying sizes, which also influenced the convergence speed, with larger network sizes generally requiring more rounds to achieve balance.

To address these challenges, this research introduces a novel algorithm, called the Adaptive Threshold Push-Pull Sum algorithm, which leverages the strengths of both the Continuous Single-Proposal Deal-Agreement-Based and the Push-Pull Sum algorithms while establishing a trade-off to lessen their respective drawbacks. The newly introduced algorithm uses the mechanic of adaptive thresholding in order to prevent load transfers with low effect in error reduction, since load transfers are pricy operations. By adapting to the current state of balance of the investigated networks, this solution aims to deliver robust performance across a wide range of scenarios, effectively bridging the gap between the two algorithms.

1.3 Related Work

Nugroho et al. [1] proposed the Push-Pull Sum algorithm, which is essentially a combination of two algorithms: the Push-Sum algorithm, introduced by David Kempe, Alin Dobra, and Johannes Gehrke [2], and the Pull-Sum algorithm. The push and the pull mechanisms are directly adopted from the Push-Pull Sum algorithm. Nugroho et al. use the MSE as a metric to evaluate the performance of their algorithm, an approach that will also be followed in this thesis. Their experiments were conducted on static general graphs, and this research similarly employs static graphs.

Dinitz et al. [3] proposed two versions of the Single-Proposal Deal-Agreement-Based algorithm, as well as two variations of a multi-neighbor load balancing algorithm: a round-robin approach and a self-stabilizing load balancing algorithm. However, the only algorithms comparable to ours are the Single-Proposal Deal-Agreement-Based algorithms, which have two variations: one for the continuous setting and one for the discrete setting. The main difference between these two is that, in the continuous setting, any load may be transferred over the edges, whereas, in the discrete setting, all load transfers must involve integers. For multi-neighbor load balancing, nodes may transfer loads to several neighbors within a single round. In contrast, the Push-Pull Sum algorithm allows this only during pull actions, where a node responds to all requesting nodes by sending loads back. Additionally, the self-stabilizing and round-robin approaches are asynchronous algorithms, whereas both the Adaptive Threshold Push-Pull Sum and the Push-Pull Sum algorithms operate synchronously.

1.4 Hypothesis

The Adaptive Threshold Push-Pull Sum algorithm, which integrates key features of the Deal-Agreement-Based algorithm and the Push-Pull Sum algorithm, will demonstrate performances that are intermediate between the two in terms of MSE

reduction across six distinct network topologies. Specifically, it is expected to perform better than the Deal-Agreement-Based algorithm in high-degree networks and perform better than the Push-Pull Sum algorithm in low-degree networks, achieving a balance that improves overall adaptability and efficiency compared to both.

This hypothesis will be evaluated through a comparative analysis of MSE across six distinct topologies, some of which feature varying network sizes, to assess the algorithm's robustness and scalability in different network environments. To analyze the data trends and draw conclusions about the convergence rate, model fitting is applied as an analysis technique. Additionally, slopes will be computed for three distinct time regions—*start*, *middle*, and *end*—to provide detailed insights into the algorithm's performance at specific stages of execution.

1.5 Contribution

This study introduces a novel load balancing algorithm that combines the strengths of two established approaches: randomized load balancing and deterministic load balancing based on deal agreement. By integrating an adaptive threshold mechanism, the algorithm dynamically adjusts to the current state of the network to enhance performance. It leverages the push and pull mechanisms to facilitate convergence to a balanced state.

2 Problem Overview

The load balancing problem is defined on an undirected general graph, where each node can transfer loads to its neighboring nodes via edges to achieve a balanced network state. The problem setting and the approach to address the problem are elaborated on in this section.

2.1 Setting

Continuous and Discrete: In the continuous setting, nodes can transfer any amount of load over the edges, while in the discrete setting, all load transfers must consist of integer values.

Synchronous and Asynchronous: In the synchronous setting, the time for message delivery is constant (e.g., O(1)), whereas in the asynchronous setting, the message delivery time can be unpredictably large. However, it is possible to convert an asynchronous setting into a synchronous one by adjusting the time frame within which messages are expected to be delivered.

Static or Dynamic: Load balancing algorithms can operate in either static or dynamic graph settings. In a dynamic graph, connections between nodes may change arbitrarily between rounds. In contrast, the connections and the nodes remain the same for the static graph.

The peer-to-peer network is modeled as a static general graph, meaning the set of edges remains unchanged during the application of the load balancing algorithms. The objective of load balancing is achieved using local algorithms, where each node gathers information only from its direct neighbors. The setting is a continuous setting. Additionally, a synchronous message delivery assumption is made, with a constant delivery time, e.g., O(1). The experiments are conducted on six distinct network topologies, each comprising 2^{10} nodes.

2.2 Approach

This research consists of three steps: the design of a load balancing algorithm, the simulation phase to test its ability to balance the state of the network across different topologies, and a comparative analysis of the simulation outcomes using statistical methods. In prior research [6], the strengths and weaknesses of two distinct load balancing algorithms were identified by simulating their performance on various topologies and network sizes to test the scalability and adaptability of the algorithms to different situations. The design of the novel adaptive threshold load balancing algorithm builds upon these findings. Each simulation outcome includes 30 distinct experiments to ensure statistical significance. The results are analyzed using model fitting to identify trends in MSE reduction, with slopes calculated for different regions to assess the consistency of performance. The findings are presented in plots, accompanied by explanations that provide insights into the observed behavior of the load balancing algorithms.

3 Algorithms

This thesis examines three load balancing algorithms: the Continuous Single-Proposal Deal-Agreement-Based algorithm, the Push-Pull Sum algorithm, and the newly proposed Adaptive Threshold Push-Pull Sum algorithm. The Adaptive Threshold Push-Pull Sums structure is described, along with how it incorporates features from the first two algorithms and the rationale behind its development. The working mechanics of each algorithm are described along with pseudo-code. Furthermore, examples are provided to show how the algorithms achieve a balanced state in the network. To provide further light on the objectives of the Adaptive Threshold Push-Pull Sum method, the desired results are also described.

3.1 Characteristics

Like the graphs, load balancing algorithms may have different characteristics. These characteristics are elaborated on below:

Static and Dynamic: Load balancing algorithms can be classified as either static or dynamic algorithms. Static algorithms assign tasks to the nodes at compile time, while dynamic algorithms assign tasks at run time. The main advantage that static load balancing algorithms have over dynamic load balancing algorithms is that they do not cause any run-time overhead [7].

Stochastic and Deterministic: Stochastic load balancing algorithms rely on randomness to select load transfer partners. Deterministic load balancing algorithms, on the other hand, follow predefined distribution rules in order to make load transfers. [4]

Global and Local: Local load balancing algorithms allow nodes to transfer loads within their domain or neighbourhood, while global load balancing algorithms enable load balancing operations across the entire network [4].

Monotonic and Non-monotonic: An algorithm is considered monotonic if each load transfer is from a higher-loaded node to a less-loaded node and the maximal load in the network never increases and the minimal load never decreases [3].

Mass conservation property: Some load balancing algorithms possess the mass conservation property, which guarantees that the values will converge to the correct aggregate of the network's ground truth [1].

Anytime: An anytime algorithm can be halted at any stage during the execution, and after stoppage the state of the network is not worse than in any previous rounds. The advantage that comes with an anytime algorithm is that the network in which the load balancing algorithm with this property is applied shows more feasible states with intermediate rounds. [3]

Many of these properties are desirable for load balancing. For instance, monotonicity and the anytime property contribute to better performance and robustness, while locality reduces computational overhead. Similarly, determinism enhances the predictability and reliability of the algorithm's behavior.

3.2 Classic Push-Pull Sum Algorithm

The Push-Pull Sum algorithm as proposed in [1] requires each node to hold sum $s_{i,r}$ and weight $w_{i,r}$ values as initial information. Initially, each node's weight is set to

$w_{i,0} = 1$, and the sum of all weights is equal to the network size N at each round. The sum of all initial $s_{i,0}$ is equal to whatever the required input $x_i \in \mathbb{R}_0^+$ is, in the paper the values for the sums are uniformly distributed values between 0 and 100 [1]. The algorithm consists of three main procedures: *RequestData*, *ResponseData*, and *Aggregate*, as detailed in algorithm 3.

Each round r, except the first, begins with the *Aggregate* procedure, where each node collects messages $M_{i,r}$ sent by other nodes $\{(s_m, w_m)\}$ in the previous round $r-1$, requesting data. The nodes then update their sum and weight values as $\sum_{m \in M_{i,r}} s_m$ and $\sum_{m \in M_{i,r}} w_m$, respectively. The updated load is computed by dividing the sum by the weight. Next, each node calls the *RequestData* procedure. In this procedure, each node chooses a random neighbor node and executes a push operation, so each node sends half of its sum $\frac{s_{i,r}}{2}$ and half of its weight $\frac{w_{i,r}}{2}$ to the chosen neighbor and itself. Finally, each node executes the pull operation, which is described in the *ResponseData* procedure. Here, each node gathers the incoming requests per round r in a set $R_{i,r}$. Then, each node replies to each requesting node, including itself, by distributing half of its sum divided by the number of incoming requests $\frac{\frac{s_{i,r}}{2}}{|R_{i,r}|}$ to each requesting node.

Algorithm 1 Push-Pull Sum algorithm

1: **procedure** RequestData
2: Chose a random neighbor node v
3: Send $(\frac{s_{u,r}}{2}, \frac{w_{u,r}}{2})$ to the chosen node v and the node u itself
4: **end procedure**
5: **procedure** ResponseData
6: $R_{u,r} \leftarrow$ Set of the nodes calling u at a round r
7: **for all** $i \in R_{u,r}$ **do**
8: Reply to i with $\left(\frac{\frac{s_{u,r}}{2}}{|R_{u,r}|}, \frac{\frac{w_{u,r}}{2}}{|R_{u,r}|}\right)$
9: **end for**
10: **end procedure**
11: **procedure** Aggregate
12: $M_{u,r} \leftarrow \{(s_m, w_m)\}$ messages sent to u at a round $r-1$
13: $s_{u,r} \leftarrow \sum_{m \in M_{u,r}} s_m, w_{u,r} \leftarrow \sum_{m \in M_{u,r}} w_m$
14: $f_{avg} \leftarrow \frac{s_{u,r}}{w_{u,r}}$
15: **end procedure**

The setting in [1] is similar to ours. While their study focuses on a Complete graph with 10^4 nodes, this study examines network sizes of 2^{10} nodes and includes different topologies. In that paper, 50 experiments were conducted, each running for 30 rounds. Their findings demonstrated that the Push-Pull Sum algorithm reduces the expected potential Φ_r exponentially. The potential function for the Complete graph is defined as:

$$\Phi_r = \sum_{i,j} \left(v_{i,j,r} - \frac{w_{i,r}}{n} \right)^2, \tag{1}$$

where the $v_{i,j,r}$ component stores the fractional value of node j's contribution at round r. The equation:

$$\mathbb{E}[\Phi_r + 1 | \Phi_r = \phi] = (\frac{2e-1}{4e} - \frac{1}{4n})\phi \tag{2}$$

is the conditional expectation of $\Phi_r + 1$ for the Push-Pull Sum algorithm. The Push-Pull Sum algorithm holds the mass-conservation property and is classified as a stochastic load balancing algorithm due to its randomized neighbor selection process [1].

The Push-Pull Sum algorithm performed very well on Complete graphs, Ring of Cliques with large clique size, Lollipop graphs with large clique size, and Star graphs. In the case of the Star graph the internal node acts as a distributor of the load. Since each leaf chooses the internal node with 100% possibility as a "random" neighbor the internal node is involved as a endpoint of $N-1$ external push operations, and redistributes the load via pull operations to the leaves, where the sum is $\frac{\frac{s_{i,r}}{2}}{N-1}$ and accordingly the weight is $\frac{\frac{w_{i,r}}{2}}{N-1}$. For for the Complete graph, the Ring of Cliques and the Lollipop graph, the density of the graph plays an crucial role. Since nodes select neighbors randomly, the high edge density allows the algorithm to spread loads efficiently, preventing bottlenecks and reducing reliance on deterministic paths. This explains why the Push-Pull Sum algorithm underperformed on Torus Grid and

Ring graphs compared to the Single-Proposal Deal-Agreement-Based algorithm, as they are limited to a degree of 4 and 2 respectively. For these topologies redundant communication may occur, as two nodes may push back and fourth, with the sum being $\frac{s_{i,r}}{2}$ and the weight being $\frac{w_{i,r}}{2}$ for the push and pull operations. The result of this action is that their load values interact in such a way that one node u adopts the previous round's state of another node v, leading to:

$$load_r(u) = load_{r-1}(v) \tag{3}$$

and vice versa. This phenomenon is described in chapter 9. $load_r(u)$ represents the load of node u at round r.

3.2.1 Example

The example in figure 2 illustrates a execution of the Push-Pull Sum algorithm on a Complete graph K_4 with 4 nodes labeled *A, B, C* and *D*. Each node is initially assigned a sum and a weight value. The undirected graph represents the network topology, showing connections between neighboring nodes.The solid directed edges depict the push operations and the dashed directed edges visualize the pull operations. Each node maintains a set $R_{i,r}$ where i is the node ID and r is the round being examined. The load of the node is calculated by $\frac{s_{i,r}}{w_{i,r}}$. The example depicts the first round of a execution of the Push-Pull Sum algorithm. The push and pull operations are distinct. The left-hand side of figure 2 depicts the behaviour of the nodes while executing the push operations, while the right side illustrates the pull operations. During the push phase, each node randomly selects a neighbor to transfer load to. In this example:

- Node A selects node C and pushes half of its sum and weight to both node C and itself. (Self-loops are omitted from the figure for readability.)

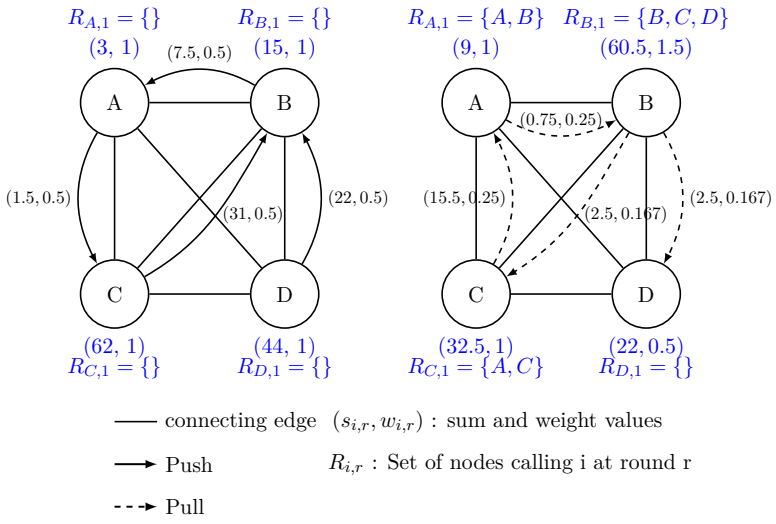

Figure 2: Push-Pull Sum: push and pull actions

- Node B selects node A as its trading partner.
- Nodes C and D push their values to node B and themselves.

Given the push operations for each node, the set $R_{i,r}$ is computed. Since node B pushed load to node A and node A pushed load to itself, we get $R_{A,1} = \{A, B\}$. The updated sum and weight values after the push phase can be inspected on the right-hand side of figure 2.

Following the push actions, each node proceeds with the *ResponseData*-procedure, executing the pull phase. Each node in $R_{i,1}$ receives a response based on the respective pull values. Since node A has two nodes in its set $R_{A,1}$, it responds to both node B and itself with $\left(\frac{\frac{3}{2}}{2}, \frac{\frac{1}{2}}{2}\right)$, as indicated by a dashed directed edge. Similarly, the remaining nodes *B, C, and D* execute their responsive pull operations. Following the push and pull operations, the nodes update their sum and weight values. The state of the network after round one is depicted in figure 3. The MSE at the beginning of round 1 is 542.50. After applying one round of the Push-Pull Sum algorithm, the MSE is reduced to 63.49.

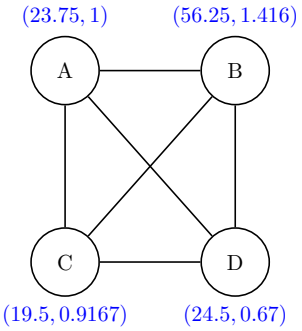

Figure 3: Push-Pull Sum: setting after round 1

3.3 Continunous Single-Proposal Deal-Agreement-Based Algorithm

The Continuous Single-Proposal Deal-Agreement-Based algorithm proposed by [3] is unlike the Push-Pull Sum algorithm, which is not a diffusion-based algorithm. The goal of load balancing is achieved based on deterministic deal agreements, where one node proposes a load to one neighboring node, and the neighboring node either accepts the transfer proposal either fully or partially. Dinitz et al. proved that the algorithm has the anytime property, meaning it never worsens the state of the network during execution. Their study examined the algorithm in a dynamic setting, where each node has access to a set of neighboring nodes, including the node's. The algorithm is divided into three phases: *proposal*, *deal*, and *summary*. In the *proposal*-phase, each node u identifies its minimally loaded neighbor v and sends a proposal to that neighbor if v has a lower load. The proposal is of value

$$\frac{load_r(u) - load_r(v)}{2} \tag{4}$$

which is labeled as a *fair* proposal. Since the load transfer is fair, the resulting load of u is not lower than that of v. In the *deal* phase, nodes evaluate the deals proposed to them. A node accepts the deal of the node that proposes the maximal load transfer. The actual transfer happens, and the load values of the nodes update their loads.

Finally, in the *summary* phase, each node informs their neighbors regarding their updated load values. [3]

Algorithm 2 Continuous Single-Proposal Deal-Agreement-Based algorithm

Input: An undirected graph $G = (V, E, load)$
Output: A load state with discrepancy at most ϵ on G

```
1:  for r = 1 and on do
2:      for every node u do
3:          Find a neighbor, v, with the minimal load
4:          if load_r(u) − load_r(v) > 0 then
5:              u sends to v a transfer proposal of value (load_r(u) − load_r(v))/2
6:          end if
7:      end for
8:      for every node u do
9:          if there is at least one transfer proposal to u then
10:             Find a neighbor, w, proposing to u the maximal transfer
11:             Node u makes a deal: informs node w on accepting its proposal
12:             The actual transfer from w to u is executed
13:         end if
14:     end for
15:     for every node u do
16:         Node u sends the updated value of its load to its neighbors
17:     end for
18: end for
```

The analysis in Dinitz et al.[3] is based on a potential function that measures the network. The potential for a node u is defined as

$$p(u) = (load(u) - L_{avg})^2 \tag{5}$$

where L_{avg} represents the current load average in the network. The potential for the graph $p(G)$ is defined as

$$p(G) = \sum_{u \in V} p(u), \tag{6}$$

which is the sum of all potential of each node in the graph G. Any fair load transfer of load l decreases the potential of the graph by at least $2 * l^2$. As a result of any round r of the Continuous Single-Proposal Deal-Agreement-Based algorithm, the

graph potential decreases by at least $\frac{K_r^2}{2D_r}$, where K is the initial discrepancy and D is a bound for the graph diameter. [3]

The Single-Proposal Deal-Agreement-Based load balancing algorithm struggles to reduce the MSE as rapidly as the Push-Pull Sum algorithm for dense graphs like the Complete graph, the Lollipop graph with a large clique size, and the Ring of Cliques with a large clique size. This limitation arises because each node seeks the minimally loaded partner for load transfer. For a Complete graph, the minimal load partner is the same node with loads of L_{min} (the minimally loaded node in the network). This causes each node to propose to the same node, which then evaluates the proposals and accepts exactly one transfer proposal, namely the maximal one. A similar scenario occurs in the Ring of Cliques and the Lollipop graph. However, in the Ring of Cliques, nodes do not all propose to the same minimal neighbor; instead, they propose to the least-loaded neighbor within their respective cliques. For the Lollipop graph, the nodes in the path graph balance their loads more quickly than the nodes in the clique, which is a bottleneck in this scenario. For the Torus Grid and the Ring graph, the Deal-Agreement-Based algorithm performs better in reducing the error. In these scenarios, the proposals are more evenly distributed among nodes due to the lower density of the graphs, allowing a greater number of nodes to participate in load transfers. The Star graph is an exception to this case, since we have a similar bottleneck as in the Complete graph, since the internal node is the common neighbor for each leaf, and thus each leaf proposes a load to the internal node. The internal node can accept only one proposal. The simulation results in the student project [6] indicate the performances of each load balancing algorithm for each topology very clearly.

3.3.1 Example

Figure 4 illustrates two settings. The left-hand side of the figure depicts the initial state and the right-handside illustrates the state after one round of execution. The

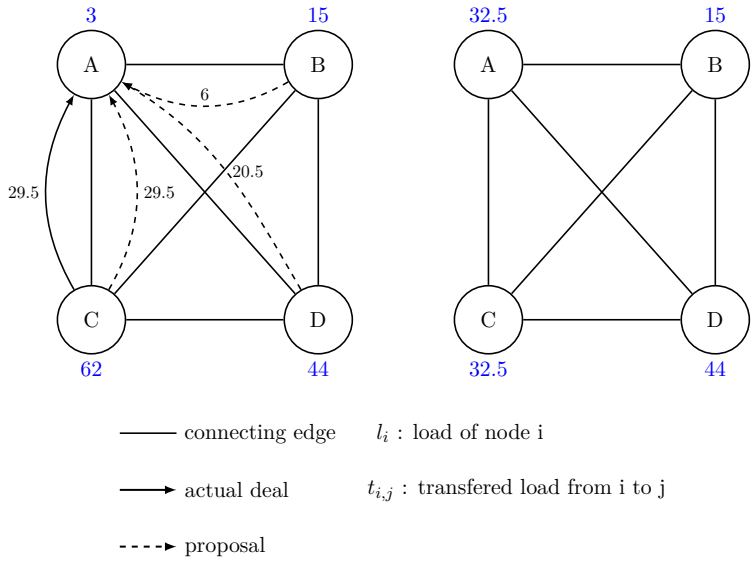

Figure 4: Deal-Agreement-Based: initial setup and setup after round 1

setting is the same as in the example above in the Push-Pull Sum section, with the difference that each node is assigned a load value, instead of sum and weight values. In the figure, dashed directed edges represent transfer proposals from one node to another, while solid directed edges indicate actual load transfers. The network consists of four nodes, labeled *A, B, C,* and *D*. Each node identifies its least-loaded neighbor as a potential transfer recipient. Nodes *B, C* and *D* determine node *A* as their minimal loaded neighbors. Node *A* identifies node *B* as the neighbor with the minimal load in its neighbourhood, however node *B* has more load than node *A*, so node *A* does not send an transfer proposal to node *B*. As a result, nodes *B, C* and *D* each send a transfer proposal of value $\frac{(load_r(i)-load_r(A))}{2}$ to node *A*, where $i \in \{B, C, D\}$. Node *A* evaluates the proposal and accepts node *C*'s transfer proposal, as node *C* proposes the largest amount of load, namely 29.5. The actual transfer happens and 29.5 of loads are transfered from node *C* to node *A*. The right-hand side of figure 4 shows the state of the network after round 1 of executing the Deal-Agreement-Based algorithm. Node *A* and *C* each have equal loads of 32.5, the loads of nodes *B* and *D* remain unchanged. The MSE at the beginning of round 1 is at 542.5. After executing the first round of the algorithm the MSE decreases to

a value of 107.375, which is approximately one-fifth of the initial MSE.

3.4 Adaptive Threshold Push-Pull Sum Algorithm

The Adaptive Threshold Push-Pull Sum algorithm is composed of key elements from both the Push-Pull Sum and Single-Proposal Deal-Agreement-Based algorithms, extended by the idea of adaptive thresholding. The Adaptive Threshold Push-Pull Sum consists of different procedures. In the *CheckThresholdsRequestData*, each node u chooses a subset $RN_{u,r}$ of

$$RN_{u,r} = \log_2 (|neighbourhood_u|) \tag{7}$$

random neighbors. This increases the likelihood of selecting a well-suited neighbor for load transfer. Selecting only one random neighbor lowers the chance to find an optimal or good neighbor to execute a load transfer. Then the load difference between the node u and each node in $RN_{u,r}$ is computed and checked against a threshold θ. The threshold is computed in the *CalculateThresholds*-procedure. The threshold θ is calculated as

$$\theta = k * \sqrt{MSE_r - 1} \tag{8}$$

where k is some factor to adjust the sensitivity of the threshold. A larger k makes the threshold more sensitive, meaning that fewer nodes are eligible for load transfer, allowing only significant load transfer. Respectively, a smaller k makes the threshold less strict; thus, more nodes are eligible for load transfers. This condition ensures that only load transfers with meaningful impact happen, and load transfers between nodes with low impact on the balance of the network are avoided. The first eligible node in $RN_{u,r}$ that exceeds the threshold receives the sum of value ($\frac{s_{i,r}}{2}$) and the weight of value ($\frac{w_{i,r}}{2}$). The *ResponseData* and the *Aggregate*-procedure are directly adapted from the Push-Pull Sum algorithm. The way the loads are distributed,

namely the push and the pull mechanisms, is directly taken from the Push-Pull Sum algorithm and extended by an adaptive threshold mechanism. Like the Single-Proposal Deal-Agreement-Based algorithm, the Adaptive Threshold Push-Pull Sum algorithm employs conditional load transfers, but with a threshold θ instead of requiring a strictly positive load difference. Instead of initiating a load transfer with the maximally proposing node, the Adaptive Threshold Push-Pull Sum algorithm orders the nodes to initiate a load transfer with the first node proposing load. The reason for that is to reduce computational overhead by avoiding that each node looks through its whole set RN and is required to evaluate each proposal. So the first node proposing a load transfer is accepted as a transfer partner.

Although formally not shown, the Adaptive Threshold Push-Pull Sum algorithm is expected to hold the mass conservation property, as it converged to the correct ground truth in all experiment settings, similar to the Push-Pull Sum algorithm. Also, given that the push and pull mechanisms are directly adapted, these operations are the only operations that let nodes transfer or receive nodes in the algorithm. The Adaptive Threhsold Push-Pull Sum algorithm inherits is an stochastic algorithm as it inherits its stochastic nature from the Push-Pull Sum algorithm, by choosing a subset of neighbors randomly.

3.4.1 Example

Figure 5 depicts a similar setting as described in section 3.2.1. According to the Adaptive Threshold Push-Pull Sum algorithm, each node chooses $\log_2(|neighbourhood|)$ neighbors. For this setting, each node chooses 2 neighbors, which are added to the set $RN_{i,1}$ for each node i. For instance, node A computes $RN_{A,1}$ as $\{B, C\}$. The load differences between node A and nodes B and C are computed. In this example, k is set to 0.01, thus the threshold θ is given by $0.01 * \sqrt{542.5} \approx 0.23$. Since both load differences between nodes A and B and nodes A and C exceed this threshold, both nodes are eligible to propose a load transfer with node A. In this scenario, node

Algorithm 3 Adaptive Threshold Push-Pull Sum algorithm

procedure CALCULATETHRESHOLDS
  $\theta \leftarrow k * \sqrt{MSE_{r-1}}$
end procedure
procedure CHECKTRESHOLDREQUESTDATA
  $RN_{u,r} \leftarrow$ choose $\lceil \log_2 (|neighbourhood(u)|) \rceil$ random neighbor
  for every node $v_i \in RN$ **do**
    $\Delta_{u,v_i} \leftarrow |(load(u) - load(v_i))|$
    if $\Delta_{u,v} > \theta$ **then**
      Send $(\frac{s_{u,r}}{2}, \frac{w_{u,r}}{2})$ to first node v fulfilling condition and the node u itself
    end if
  end for
end procedure
procedure RESPONSEDATA
  $R_{u,r} \leftarrow$ Set of the nodes calling u at a round r
  for all $i \in R_{u,r}$ **do**
    Reply to i with $\left(\frac{\frac{s_{u,r}}{2}}{|R_{u,r}|}, \frac{\frac{w_{u,r}}{2}}{|R_{u,r}|} \right)$
  end for
end procedure
procedure AGGREGATE
  $M_{u,t} \leftarrow \{(s_m, w_m)\}$ messages sent to u at a round $r-1$
  $s_{u,t} \leftarrow \sum_{m \in M_{u,r}} s_m, w_{u,r} \leftarrow \sum_{m \in M_{u,r}} w_m$
  $load(u) \leftarrow \frac{s_{u,r}}{w_{u,r}}$
end procedure

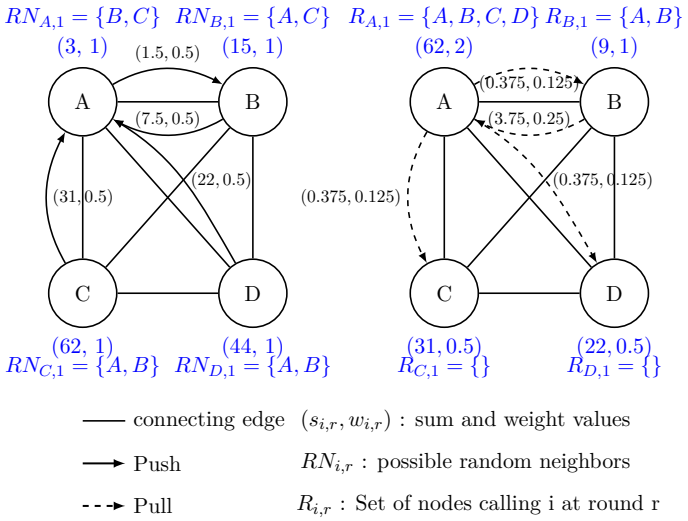

Figure 5: Adaptive Threshold Push-Pull Sum: push and pull actions

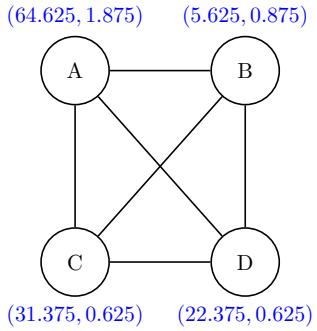

Figure 6: Adaptive Threshold Push-Pull Sum: setting after round 1

A selects node B as a transfer partner and pushes half of its sum 1.5 and weight 0.5 to node B and itself. This process is repeated for each node accordingly. Similar to the example in section 3.2.1, the nodes then execute the pull operation. The result is depicted in figure 6. The MSE dropped from 542.5 initially to 251.86. The error reduction depends on the sensitivity factor k. If k is set to 1, the load transfer between node A and B would not have happened. Instead, nodes A and C would have exchanged loads, leading to a larger impact on the balance of the network.

3.4.2 Aspired Outcome

Considering the simulation results presented in [6], the discrepancy between the MSE reduction abilities per round for the different topologies shows that the algorithms perform either very well or mediocre to bad. The primary motivation behind designing the Adaptive Threshold Push-Pull Sum algorithm was to find a compromise solution that enhances adaptability across various network topologies.

The final results of the first load balancing step can be taken from table 1. The Push-Pull Sum algorithm shows the lowest MSE after round 1, followed by the Deal-Agreement-Based algorithm and the Adaptive Threshold Push-Pull Sum algorithm. A small k value was used for demonstrative purposes (as the simulations were conducted with small k values). A higher k value would have a greater impact in the first round. In section 6, we will see that the Adaptive Threshold Push-Pull Sum algorithm

	Initial	Dinitz et al.	Nugroho et al.	Bayazitoglu
Node A	3	32.5	(23.75, 1) = 23.75	(64.625, 1.875) = 34.47
Node B	15	15	(56.25, 1.416) = 39.72	(5.625, 0.875) = 6.43
Node C	62	32.5	(19.5, 0.9167) = 21.27	(31.375, 0.625) = 50.2
Node D	44	44	(24.5, 0.67) = 36.57	(22.375, 0.625) = 35.8
MSE	542.50	107.375	63.49	251.86

Table 1: Overview over example outcomes

proceeds to enhance in reducing error in later rounds, as the MSE and thus the thresholds adjust.

4 Topologies

The simulations were conducted for six distinct network topologies. Each network has 2^{10} (1024) nodes. The behavior of the algorithms in these different topologies is observed, since each topology has different characteristics; different performances exploiting the specials of the topologies are expected. The topologies contain *Complete graph*, *Torus Grid graph*, *Ring graph*, *Star graph*, *Lollipop graph*, and *Ring of Cliques*. In the following, the topologies including these characteristics are presented.

4.1 Complete Graph

The Complete graph K_N, as illustrated in figure 7, is a graph where each pair of distinct nodes is connected by an edge. The Complete graph, also referred to as a fully connected graph, has N nodes and $\frac{N\times(N-1)}{2}$ edges. The Complete graph is a regular graph, where each node has a degree of $N-1$. As it contains the maximum possible number of edges for a given set of nodes, it is considered a dense graph [5]. The diameter of a Complete graph is 1, as each node is directly connected to every other node. Since each node has the same degree and connectivity, algorithms can treat all nodes uniformly.

The Complete graph is used in financial trading systems and military communications, where high reliability and low latency are critical. The Complete graph ensures optimal routing paths between nodes, due to its low diameter [8].

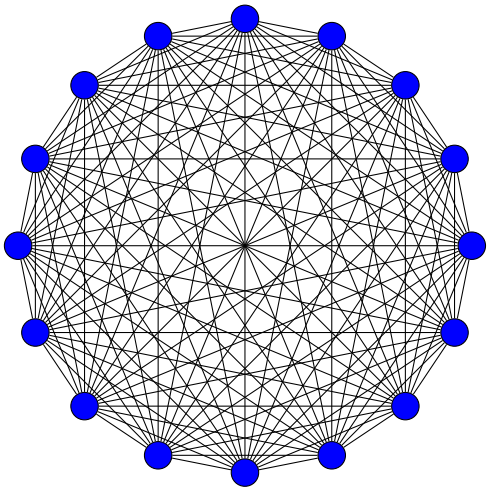

Figure 7: Complete graph: network size 16

4.2 Torus Grid Graph

The two-dimensional Torus Grid graph, also referred to as the $k \times m$-Torus graph or $T_{k,m}$, is a graph that is built like a two-dimensional mesh with wrap-around edges as depicted in figure 8 [9]. Here, k represents the height, while m denotes the width of the grid. The graph consists of $k \times m$ nodes and $2 \times k \times m$ edges (if $k, m > 2$) and is a regular graph, where each node has a degree of 4. The graph's diameter is given by $\frac{\min(k,m)}{2}$. Tori are scalable, as the number of connections per node is constant, regardless of the graph size. In the previous research [6], the simulation results showed to not vary over different network sizes. Torus topology is widely used in supercomputers like IBM Blue Gene and Cray systems for high-performance computing. It is also implemented in Network-on-Chip (NoC) designs for its ability to handle data distribution with low latency and high fault tolerance [8].

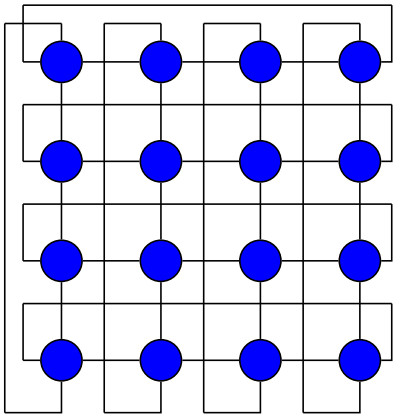

Figure 8: Torus Grid graph: network size 16

4.3 Ring Graph

The Ring graph R_N is a regular graph, where each node has a degree of two, forming a cycle. The Ring graph can be constructed by building a Path graph, where the first and the last nodes are connected by an edge as depicted in figure 9. The graph consists of N nodes and N edges. The diameter of a ring is given by $\lfloor \frac{N}{2} \rfloor$. The regularity ensures that no single node has an advantage, making algorithm design and guaranteeing fairness in load balancing easier. Most of the Ring structures use a token-based communication model. The node that holds the token may transmit data. Most of the current high-speed LANs have a Ring topology [10]. The advantage of a Ring structure is that it is easy to troubleshoot when faults occur, as the node that is faulty hinders the whole traffic. However, a significant drawback is that a single outage of a node may disrupt the whole network activity.

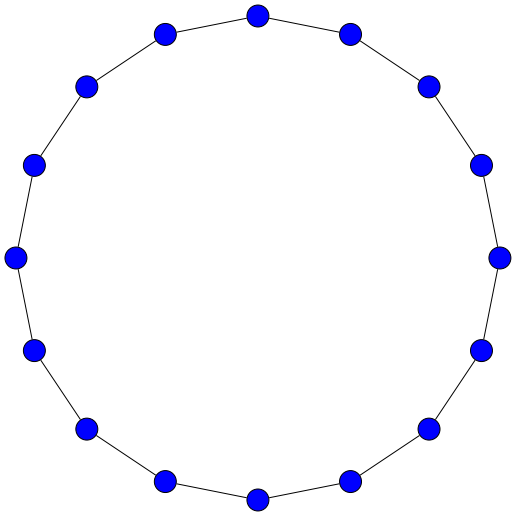

Figure 9: Ring graph: network size 16

4.4 Star Graph

A Star graph S_N as illustrated in figure 10, is a bipartite graph [11] that is structured like a tree structure with a single central node connected to $N-1$ nodes, or leaves. A Star graph with N nodes has $N-1$ edges. In this structure, every leaf node has a degree of 1, meaning it is connected only to the internal node. The central node has a degree of $N-1$. The diameter of a Star graph is 2, as the path from one leaf node through internal node to another leaf node takes two steps. From a load balancing perspective the internal node acts as a point of redistribution. This topology is particularly suitable for master-slave or client-server models where the central node delegates tasks and collects results. A challenge to face when using the Star topology is that the central node may become overloaded in high-load scenarios, requiring careful design to prevent bottlenecks. A common usage for the Star topology is a LAN (Local Area Network) in home networks, where all devices are connected to a hub or the router [12]. A drawback when dealing with Star graphs is that the failure of the central node (hub or router) shuts down the whole network. The advantage of

such a setting is that adding new devices is simple and failures of leaf nodes do not affect the whole network.

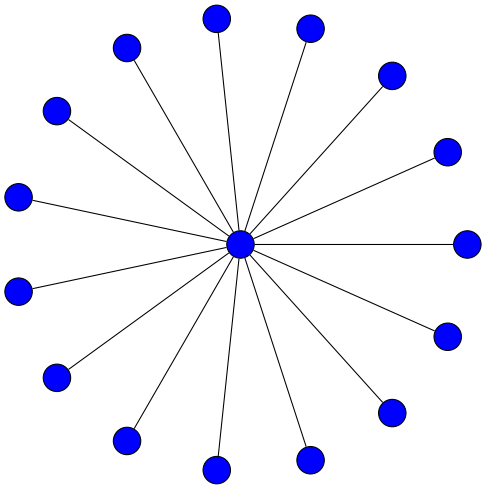

Figure 10: Star graph: network size 16

4.5 Lollipop Graph

A (k, m)-Lollipop graph $L_{k,m}$ is a graph that consists of a clique and a Path graph as depicted in figure 11. The clique and the Path graph are connected by a bridge node, thus a single edge. The (k, m)-Lollipop graph consists of a clique with k nodes and a path size of m nodes. A Lollipop graph has N nodes, where $N = k + m$ and $(\frac{k*(k-1)}{2}) + m$ edges [13].

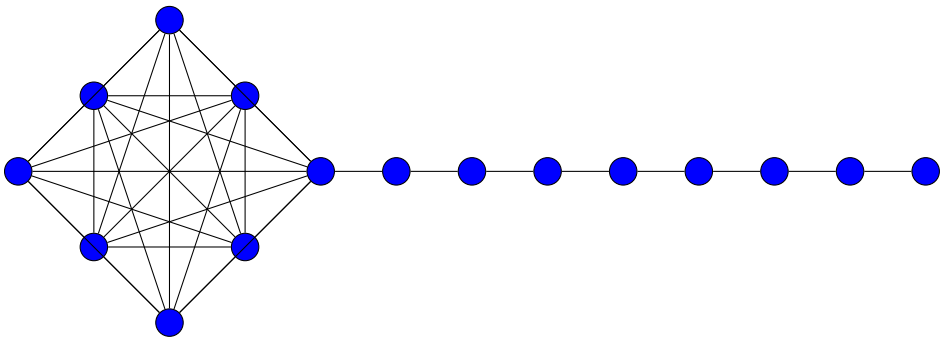

Figure 11: Lollipop graph: network size 16

4.6 Ring of Cliques

The $(k \times m)$-Ring of Cliques $ROC_{k,m}$ consists of k cliques, each containing m nodes. The cliques are connected to form a ring structure. To create the ring, one edge from each clique is removed, and the endpoints of these removed edges are connected to form a regular graph [9]. A $k \times m$ ring of cliques has $\left(k \times \left(\frac{m \times (m-1)}{2} - 1\right)\right) + k$ edges. The connectivity of the graph increases with larger clique sizes and decreases with smaller clique sizes.

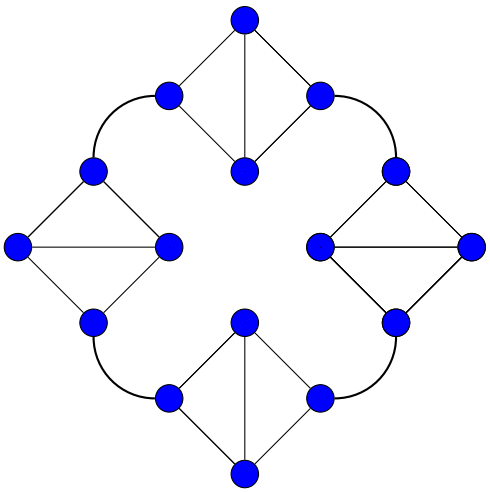

Figure 12: Ring of Cliques: network size 16

4.7 Expected Outcome

Complete graph: The high-connectivity of the Complete graph provides a variety of load transfer opportunities for each node, which will benefit randomized algoithms such as the Push-Pull Sum based load balancing algorithms, as they spread the loads uniformly across the entire network. However, the Complete graph creates a bottleneck for the Deal-Agreement-Based algorithm, as all nodes propose to the same subset of neighbors (if there are multiple nodes that hold L_{min}). Since only the highest proposal is accepted per node, the number of transfers per round is

significantly limited. **Torus Grid graph**: Many load balancing algorithms perform well on 2D Tori due to the focus on local redistribution. The wrap around edges eliminate boundary effects and provide balanced redistribution across the entire grid. Due to its low regular degree the Deal-Agreement-Based algorithm will perform very well, as the nodes distribute load efficiently between each of its four neighbors. The Adaptive Threshold Push-Pull Sum algorithm improves upon the traditional Push-Pull Sum algorithm by selecting a subset of neighboring nodes and restricting load transfers to those with significant impact on the network balance. This approach utilises smaller neighbourhoods more effectively than a purely randomized strategy. **Ring graph**: Unlike Complete graphs or Tori, the Ring graph possesses a sequential nature of data transfers, which makes it slower for loads to propagate across the entire ring. The Deal-Agreement-Based algorithm draws an important advantage over the Push-Pull Based algorithms as it chooses the optimal load transfer partner out of its two immediate neighbors. In contrast, the Push-Pull Sum-based algorithms rely on random neighbor selection, which is suboptimal in a ring structure.The Push-Pull Sum algorithm selects one of two nodes randomly, as does the Adaptive Threshold Push-Pull Sum algorithm, because each node chooses a subset of $\log_2(2)$ and ultimately ends up with one neighbor. **Star graph**: In the Star graph the central node acts as a point of redistribution. This benefits the Push-Pull Sum based algorithms, as each node pushes to the central node (for the Adaptive Threshold Push-Pull Sum algorithm, this is only the case if the load discrepancies surpass the threshold). The central node redistributes loads to each leaf. For the Deal-Agreement-Based algorithm the Star graph creates a bottleneck, since each leaf has only one neighbor (the central node), all nodes propose to the same central node. The internal neighbor initiates the load transfer, accepting the maximal proposing load, resulting in exactly one load transfer. **Lollipop graph**: The Lollipop graph is particularly interesting since it combines a dense clique structure with a sparse Path graph, which introduces a mixed topology challenge. The node linking the clique and the Path graph often becomes a bottleneck, since it bridges two different connectivity

regions. Within the clique, load balancing is highly efficient for Push-Pull Sum based algorithms, while the Deal-Agreement-Based algorithm struggles due to excessive proposals. Load transfers in the Path graph are sequential, where a deterministic approach like the one of the Deal-Agreement-Based algorithm shows to be very effective, while randomized algorithms like the Push-Pull Sum algorithm will show a moderate perforamce. The relative sizes of the clique and path affect algorithm performance, a larger clique benefits Push-Pull Sum-based approaches, while an extended Path favors the Deal-Agreement-Based algorithm. **Ring of Cliques**: Within each clique, Push-Pull Sum-based algorithms perform well due to dense intra-clique connectivity. However, inter-clique balancing poses a challenge for the Push-Pull Sum based algorithms. The Deal-Agreement-Based algorithm benefits from its deterministic load distribution, efficiently transferring loads via the bridging nodes to other cliques once internal balancing is achieved. Push-Pull Sum algorithms struggle due to randomized inter-clique communication. The Adaptive Threshold Push-Pull Sum algorithm mitigates this by selecting neighbors based on a threshold, often favoring inter-clique exchanges, once internal balancing is achieved. The shared nodes between cliques act as bottlenecks, regulating load transfer and potentially becoming overloaded.

5 Implementation and Technology Stack

A variety of technologies were utilized to achieve the underlying results. Simulations were conducted using *PeerSim*, a simulation framework for *Java*. As a result of each simulation, an output file is generated containing different simulation parameters, settings, and performance metrics. The data analysis part of this project is primarily implemented using *Python* as a programming language.

5.1 Programming Languages

Python *3.12.6* is used for several tasks, mostly for preparing and analyzing data necessary to conduct simulations and post-simulation analysis. For plotting purposes, *matplotlib v.3.9.1* is used and for handling data and data analysis *SciPy v.1.14.1* is used.

For conducting the simulations, *Java Oracle OpenJDK 21.0.1* and *PeerSim v.1.0.5* are used.

5.2 Simulation Framwork

PeerSim is a simulation tool developed in Java, which is composed of two engines: the cycle-driven engine and the event-driven engine. I chose PeerSim for our simulations

because it is well-suited for large-scale peer-to-peer simulations. In previous projects, I was able to conduct simulations up to 2^{14} nodes and could probably push the boundaries by scaling to even higher dimensions. PeerSim is designed with pluggable components, implemented as interfaces, which are intuitive to use generally. Running a simulation in PeerSim follows four steps. The first step is setting up a *configuration file*, which defines key parameters such as network size and the load-balancing protocols being simulated.

```
1  # network size declaration and initialization
2  SIZE = 1024
3  network.size SIZE
4
5  # Synchrounous CD Protocol
6  CYCLES = 100
7  simulation.cycles CYCLES
8
9  # classic PPS protocol definition
10 protocol.loadBalancingProtocols loadBalancingProtocols.
11 PushPullSumProtocol
12 protocol.loadBalancingProtocols.linkable loadBalancingProtocols
13
14 # Control classic PPS
15 control.avgo loadBalancingProtocols.PushPullSumObserver
16
17 # The protocol to operate on
18 control.avgo.protocol loadBalancingProtocols
19 control.avgo.numberOfCycles CYCLES
```

Listing 5.1: Example configuration

Listing 5.1 shows a section of a configuration file used in this project. This configura-

tion sets up a simulation of the Push-Pull Sum algorithm for a network with 1024 nodes (**lines 2 and 3**) for 100 rounds (**lines 6 and 7** in Listing 5.1). From **lines 10 to 12**, the Push-Pull Sum algorithm is loaded. The way the algorithms are implemented, one algorithm consists of at least two Java classes, the *<ProtocolName>Protocol.java* and the *<ProtocolName>Observer*, and a shared *loadBalancingParameters*-class, which contains parameters like the cycle counter or topology-specific parameters as depicted in figure 13. At **line 15**, the *control* class is declared, and its usage follows in **lines 18 and 19**, where it is assigned parameters of type *protocol* and *numberOfCycles*. This process simultaneously handles steps two and three of creating a simulation by selecting the protocols to simulate and specifying control objects. Following that, the last step is to invoke the simulator class *peersim.Simulator.class*. For that, the IDE may be configured to call the simulator class on execution of the program code. Alternatively, a command line in the terminal can also invoke the simulator class. More on this in the PeerSim documentation [14].

PeerSim provides a wide range of classes and interfaces for simulations. In the cycle-driven approach, the framework offers the *CDProtocol* interface, which defines the *nextCycle* method. The *nextCycle* method is executed at the beginning of every simulation round.

Nodes in PeerSim are implemented as containers that hold various protocols. Each node is uniquely identified by a *nodeID* and interacts with the *Linkable* interface, which provides access to neighboring nodes. A class implementing the Linkable interface can override several methods, such as:

- **getNeighbor()**: Retrieves a neighbor with a specified ID.
- **degree()**: Returns the number of connections (or neighbors) a node has.
- **addNeighbor()**: Adds a neighbor to the node's set of neighbors.

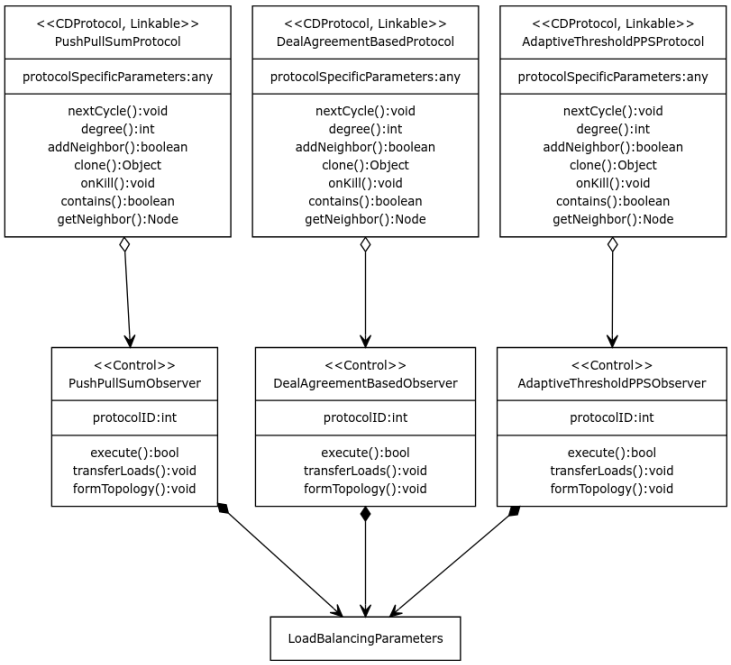

Figure 13: Project structure

To monitor or modify simulations, control objects are required. A class implementing the *Control* interface must define the execute method, which can be used to observe or alter the simulation at each round. [14]

5.3 Implementation Details

Figure 14 depicts a process model, modeling the method chosen to transition from experiment creation to data analysis and visualization. The methodology follows three steps. First, I wrote a Python script that generates configuration files where each node has uniformly distributed random load/sum values. 30 distinct experiments were created to improve statistical significance. Then a Java script reads these configuration files and assigns an initial load value to each node. Then the simulations are conducted. Each simulation outputs a file containing the simulation results, mainly the MSE per round, the loads per round, and the configuration of the network (e.g., which

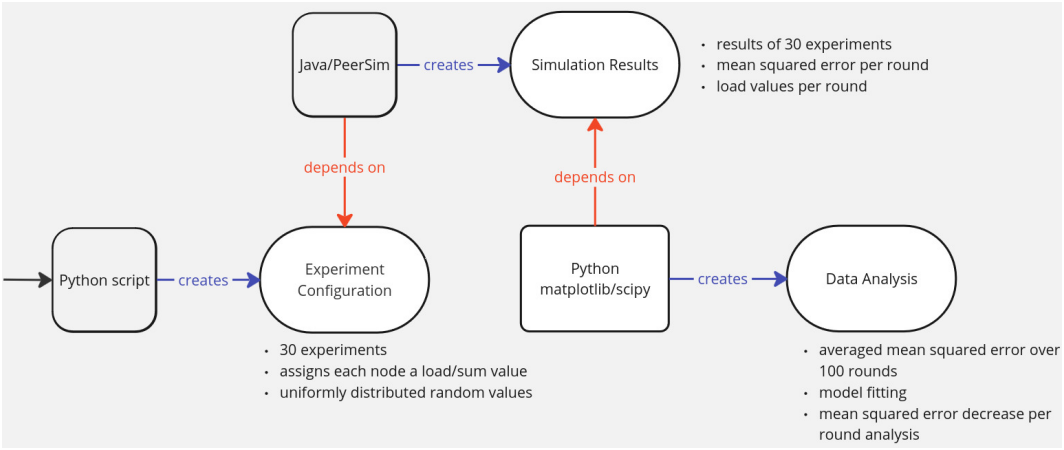

Figure 14: Process model: methodic

topology is chosen, network size, etc.). The simulation results are averaged per round and then analyzed. Out of the simulation results, plots are generated, showing the MSE reduction per round in log-log or log-linear graphs. Additionally, model-fitting techniques are applied to further analyze trends in the data.

6 Simulation Outcomes

When analyzing load balancing algorithms, the stability and efficiency of the algorithms are considered. Stability refers to how well an algorithm balances any initial load distribution across a network [4]. In the following, this is tested. 1. by conducting 30 independent experiments for each topology, each with different initial load values per node 2. by choosing six distinct topologies (some with varying structural symmetry, e.g., $L_{32,32}$, $L_{128,8}$, and $L_{8,128}$) to test the performance of the load balancing algorithms. Efficiency measures how fast an algorithm achieves a balanced state in the network. To test this, the MSE is chosen as a metric and compared over the rounds to see which algorithm achieves low error values faster. A lower MSE at an earlier stage indicates higher efficiency. For clarity, the load balancing algorithms are abbreviated:

DAB - Single-Proposal Deal-Agreement-Based Algorithm

PPS - Push-Pull Sum Algorithm (classic or traditional PPS)

ATPPS - Adaptive Threshold Push-Pull Sum Algorithm (adaptive PPS)

The simulation outcomes are presented in log-log or log-linear graphs (logs for the MSE data are base 10), since the MSE varies significantly over the 100 simulation rounds. Each simulation outcome includes an analysis of the slopes for three regions of the x-axis (simulation rounds) and the overall slope computed across all 100 rounds. The slopes are computed in either the log-log representation or the log-linear

representation. The log-log representation helps analyze power-law relationships of form

$$MSE_r = a * r^b, \tag{9}$$

where relative changes matter more than absolute differences. A slope of b means that a 1% increase in r leads to a b% increase in MSE. A slope greater than 1 indicates that the MSE increases faster than r. A slope between 0 and 1 means the MSE increases slower than r. A negative slope indicates that the MSE decreases as r increases. When dealing with exponential trends, where absolute changes in r lead to multiplicative changes in MSE. A slope of b means that each unit increase in r scales MSE by a factor of e^b. The slopes of the log-log representation is calculated as:

$$(\frac{\log_{10} MSE_{r_2} - \log_{10} MSE_{r_1}}{\log_{10} r_2 - \log_{10} r_1}). \tag{10}$$

The slopes for the log-linear representation is calculated as:

$$(\frac{\log_{10} MSE_{r_2} - \log_{10} MSE_{r_1}}{r_2 - r_1}) \tag{11}$$

[15]. The MSE data over time is modeled using linear regression, polynomial regression, exponential regression, or logarithmic regression, depending on the best-fitting model.

Linear Regression: Linear regression models the relationship between MSE and simulation rounds as

$$MSE_r = m * r + b, \tag{12}$$

where m is the slope, calculated as $m = \frac{\Delta MSE}{\Delta r} = (\frac{MSE_{r_2} - MSE_{r_1}}{r_2 - r_1})$. In this context the slope is mostly negative, as MSE_r decreases in comparison to MSE_{r-1}. b is the initial MSE at round $r = 0$, which represents the initial imbalance of the network

before any load balancing is applied.

Polynomial Regression: The polynomial regression model is expressed as

$$MSE_r = a_0 + a_1 * r + a_2 * r^2 + a_3 * r^3 + ... + a_n * r^n. \tag{13}$$

This model is utilized when MSE reduction per round follows a power law relationship. It captures non-linear relationships between the independent variable r and dependent variable MSE_r [16]. Polynomial regression can model non-linear trends like diminishing returns (e.g., rapid MSE reduction initially, then slower reduction). It fits the curvature of MSE decay, even if it's not strictly exponential or linear. Higher-degree polynomials can capture intricate patterns in the reduction of MSE over rounds.

Exponential Regression: The exponential regression model is given by

$$MSE_r = a * e^{-br}. \tag{14}$$

Exponential models capture the initially steep drop in MSE at early rounds, followed by slower reductions in later rounds. a represents the initial MSE value. A larger a indicates a higher initial load imbalance in the network. b is the decay rate; it captures how quickly the MSE decreases per round r. Since MSE decreases over time, b is negative. A larger negative value for b indicates a faster error reduction in the network, thus a faster convergence, while values closer to 0 indicate slower error reduction.

Logarithmic Regression: The logarithmic regression models data as

$$\log(MSE_r) = a + b * \log(r), \tag{15}$$

where a is the initial MSE when $\log(r) = 0$ and b is the rate of reduction per unit increase in $\log(r)$. A large positive b decreases the MSE faster. If b is small, the error

reduction slows down as the rounds progress. This model is effective in analyzing load balancing algorithms where initial rounds see significant MSE reductions, followed by progressively smaller improvements.

6.1 Complete Graph

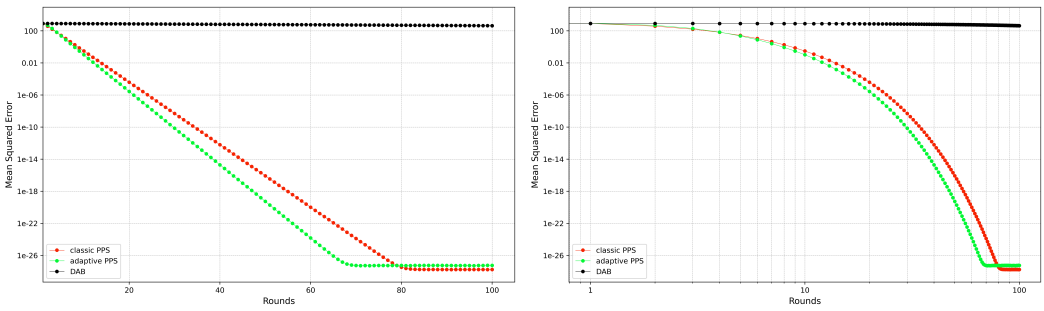

(a) **(b)**

Figure 15: Complete graph: mean squared error per rounds (log-linear and log-log)

Figure 15 a) presents the MSE reduction per round for the three load balancing algorithms simulated on the Complete graph on a log-linear graph. Figure 15 b) shows the log-log graph of the same. The DAB curve (black curve) shows a linear trend and a gentle decrease of the MSE over the 100 rounds. The DAB performs poorly since it uses a fixed, deterministic load redistribution rule for its nodes, where each node selects the minimally loaded neighbor and proposes a load transfer. In a Complete graph where each node is interconnected, the same few nodes that hold the load of amount L_{min} are the nodes that are receiving all the proposals. Since each minimal neighbor only accepts one proposal per round, the number of load transfers is heavily limited, resulting in slow MSE reduction. The PPS and ATPPS algorithms leverage the high connectivity of the network more effectively, due to their randomized nature. The PPS curve (red curve) exhibits a steady decrease in MSE, therefore showing efficient MSE reduction over time. Since all nodes are equally connected, no structural constraints slow down the process

of pushing and pulling loads from neighbors. However, PPS does not distinguish between nodes that are highly imbalanced and those that are nearly balanced, leading to unnecessary load transfers in later rounds, which slows convergence. The ATPPS algorithm (green curve) achieves even faster MSE reduction than PPS. As the system nears equilibrium, ATPPS reduces redundant exchanges. The stagnation at around 1.8×10^{19} (2^{64}) in the simulation is due to the limitations of Java's double precision, which cannot represent all integers exactly beyond a threshold. As a result, small increments become too insignificant to alter the MSE value, causing stagnation. In summary, DAB underperforms due to limitations on the amount of load transfers; PPS improves upon this but lacks adaptive control, while ATPPS optimally balances load while avoiding unnecessary exchanges, making it the most effective approach in this setting.

Figure 16 a) shows the linear regression fit for the MSE data of the DAB algorithm. The data aligns well with the model, but the exponential regression fit suits better in this case. Figure 16 b) shows the exponential regression fit for the MSE data when the DAB algorithm as a load balancing algorithm is applied to the network. Even though the curve might not suggest an exponential decay, the MSE data fits with the exponential regression model following the equation

$$MSE_r = 844.63 * e^{-0.01*r}. \tag{16}$$

The decay rate of -0.01 suggests a very slow decrease in MSE. The fitted curve and model seem very suitable for the MSE data, since the fitted curve aligns with the MSE data. The MSE data of the PPS is fitted to the exponential regression model for rounds 10 to 80. Over time, randomized exchanges smooth out load imbalances, leading to an exponential decay in MSE, as seen in figure 17. The best fit follows the equation

$$MSE_r = 2530.41 * e^{-0.9*r}. \tag{17}$$

Compared the decay rate of -0.9 suggests a steeper decline in error. In Figure 18, the exponential regression fit is visualized for the MSE data of the ATPPS load balancing algorithm graph in the Complete graph for rounds 10 to 65. The fitted curve is expressed by the equation

$$MSE_r = 4309.94 * e^{-1.06*r}. \tag{18}$$

A steep error reduction is indicated by the decay rate of -1.06. As the PPS algorithm, the ATPPS algorithm reduces the error very effectively in an exponential manner. Rounds 66 to 100 show a plateauing of the MSE data, caused by precision problems of the double datatype in Java. The adaptive mechanism provides a faster decline in error indicated by the decay rate of -1.06 versus the one of the PPS of -0.9.

Figure 19 visualizes a heat map of the slopes in both the log-linear a) and log-log b) representations for the three load balancing algorithms across different regions of the graph. The values reflect how steeply the MSE decreases over rounds. In the start region (rounds 1 to 10), PPS and ATPPS achieve a decay rate of -0.38 and -0.43, while DAB only reaches a value of -2.6×10^{-3}. In the early phase, PPS and ATPPS have a much faster exponential decay in MSE than DAB, meaning they reduce error more effectively at the start. In the middle region (rounds 11 to 65), the PPS and ATPPS slightly accelerate the error reduction to -0.39 for the PPS and -0.46 for the ATPPS. DAB proceeds to reduce the error in a slow manner. The decay rate is as low as -2.7×10^{-3} for the DAB. DAB has shallower negative slopes overall, which shows a more gradual and consistently slow error reduction across all regions. The stagnation behaviour described above can also be seen in the decay rate, which is close to zero in the final region, i.e. precisely when the ATPPS curve begins to stagnate. The PPS curve does not stagnate until round 80, so the decay rate is still relatively high. The general decay rates (rounds 1-100) for PPS and ATPPS (-0.3) are steeper than DAB (-2.8×10^{-3}), which suggests that PPS and ATPPS converge much faster on average. The MSE is reduced significantly by the PPS and ATPPS.

The initial MSE value of 832 is reduced to 1.72×10^{-28} for the PPS and 5.63×10^{-28} for the ATPPS, while the DAB reduced the error to nearly half of the initial value, achieving a value of 436.84.

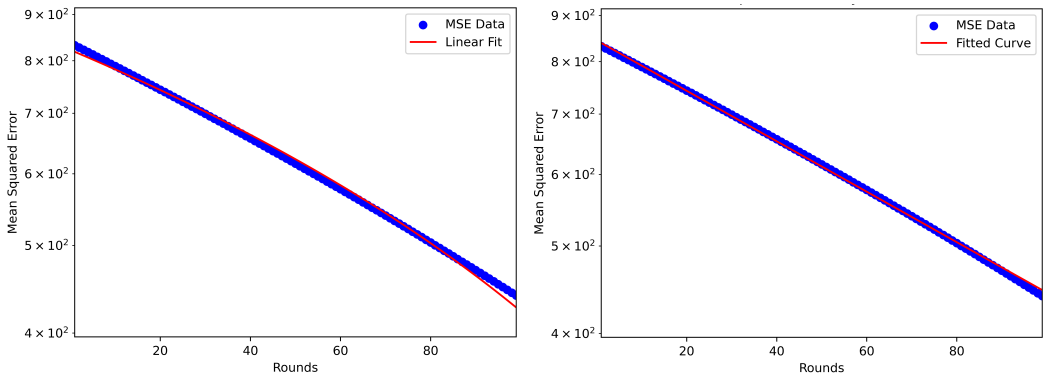

(a) **(b)**

Figure 16: Complete graph - linear and exponential regression

6.2 Star Graph

The behavior of the curves in figure 20 is similar to those for the Complete graph, with the difference that the PPS curve falls more steeply than the ATPPS curve. Figure 20 a) shows the log-linear representation of the MSE data, while figure 20 b) shows the log-log representation. Again, DAB shows a much slower MSE reduction compared to PPS and ATPPS, as indicated by the flatter slope of its curve. It converges minimally, with MSE reducing in a slow manner over rounds. This indicates that DAB is less efficient in balancing load in a Star graph, likely due to its deterministic nature and lack of dynamic adaptability. In the Star graph, all the leaves have the central node as a neighbor, meaning each leaf node selects the same central node to propose load transfers. When the central node has a higher load than the leaf requesting a transfer, no load transfer occurs between these two nodes, creating a bottleneck. Both PPS and ATPPS exhibit steep MSE reductions early on, as seen in the sharp downward trends in the log-log plot. The PPS algorithm balances load

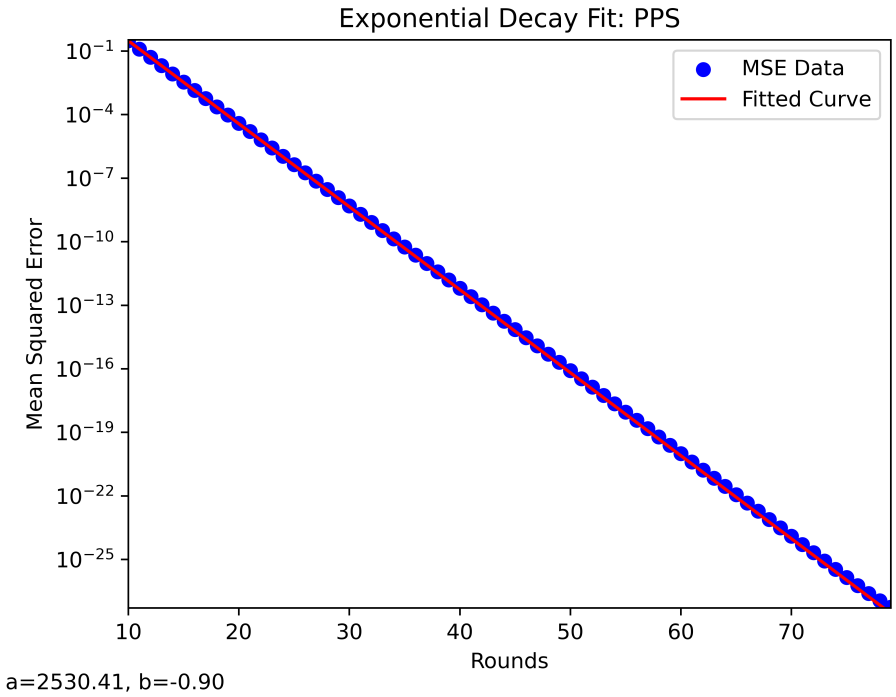

Figure 17: Complete graph - exponential regression fit: PPS

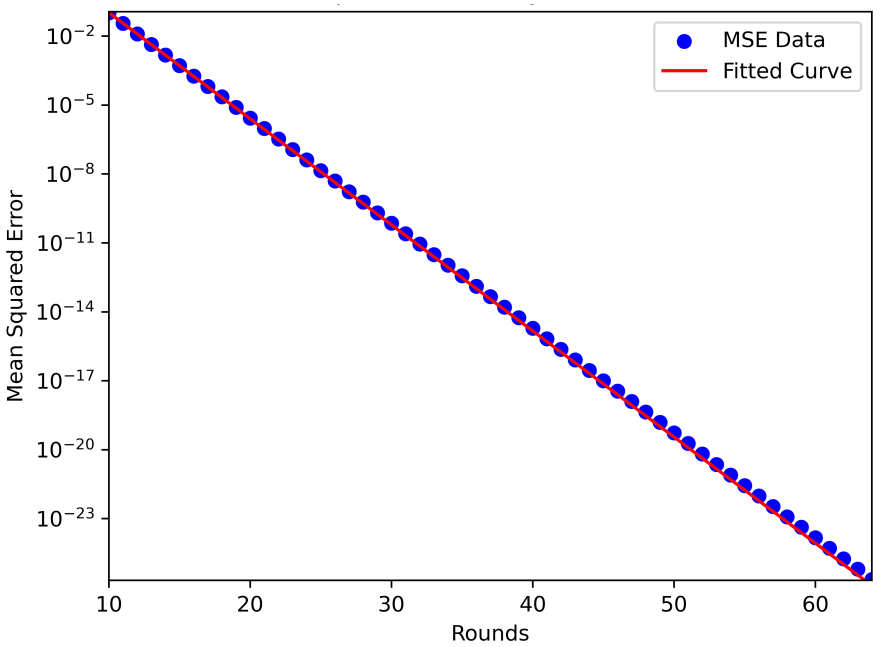

Figure 18: Complete graph - exponential regression fit: ATPPS

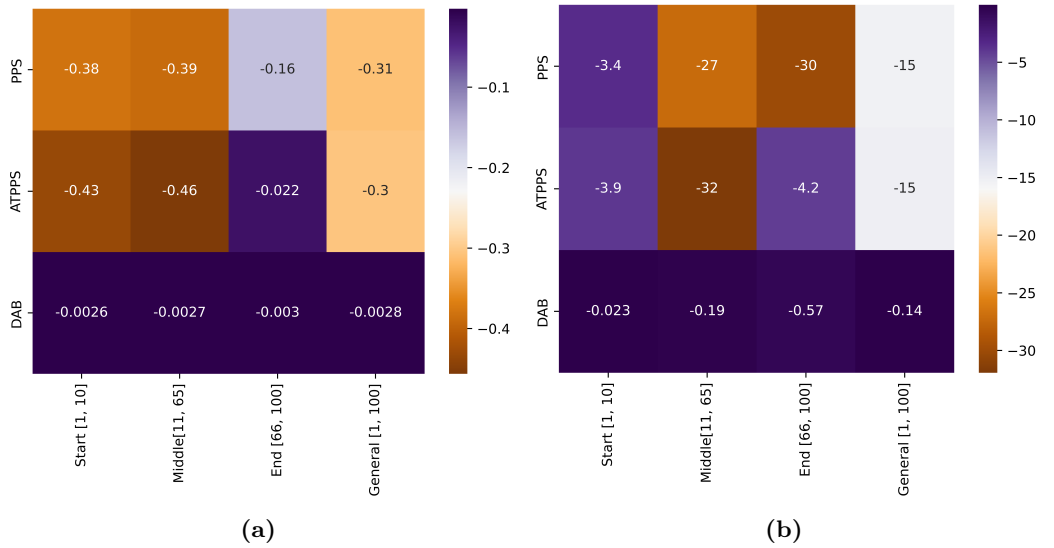

(a) **(b)**

Figure 19: Complete graph: heat map of slopes per region - log-linear and log-log

more efficiently than the ATPPS algorithm since it reduces MSE faster and reaches lower MSE values sooner (as of round 45). Again, the PPS and ATPPS curves start to plateau, as a result of the precision of double. The Push-Pull Sum based algorithms draw an advantage from the Star graph, as the redistribution happens through the central node, which is chosen by every leaf node as a push destination. Following that, the central node redistributes parts of the load to the leaf nodes in magnitude of $\frac{\frac{s_i,r}{2}}{N-1}$.

As seen in figure 21 b) the MSE data for the DAB-balanced network aligns nearly perfectly with the fitted curve of the exponential regression model given by the equation

$$MSE_r = 840.42 * e^{-0.01*r} \tag{19}$$

for the rounds 1 to 100. The decay rate of -0.01 indicates a very slow reduction in error. Since a linear decrease is suspected, the MSE data is also fitted to the linear regression model as presented in 21 a). However, the exponential regression model

aligns better with the DAB MSE data. From round to round, the improvement in the network remains minimal. This highlights the inability of the DAB to balance the network within 100 rounds to a satisfactory level. Figures 22 and 23 show the fitted curves for the MSE data of the PPS and ATPPS algorithms, respectively. The best-fit model for the MSE data of the PPS load balancing algorithm between rounds 10 to 45 follows the equation

$$MSE_r = 29794.60 * e^{-1.39*r}. \tag{20}$$

The rounds 10 to 45 exhibit the steepest decline in MSE, and for that reason, they have been fitted to an exponential regression model. The decay rate of -1.39 indicates a rapid reduction in error, especially in comparison to DAB. For the ATPPS algorithm, the MSE data fits best with the exponential model in the range of rounds 18 to 60, following the equation

$$MSE_r = 9329.40 * e^{-1.05*r}. \tag{21}$$

In Star graphs, the central node dominates communication, and load balancing heavily depends on that node. Threshold-based adjustments do not significantly impact performance under these conditions. The discrepancy between the two PPS algorithms can be explained by the fact that the ATPPS limits the number of messages due to the conditional threshold-based load transfer, which means that there is less interaction compared to the PPS.

Overall, the situation is similar to the Complete graph, with the Push-Pull Sum-based algorithms performing an extremely quick error reduction and the DAB reducing the error exponentially at a very slow rate. This behavior is captured in the heat map of figure 24, where both trends: log-linear a) and log-log b) are presented. In the first 10 rounds, the PPS achieves the fastest decay with a decay rate of -0.5, followed by the ATPPS with a decay rate of -0.45. The DAB experiences a very slow decay with a value of -2.3×10^{-3}. Between rounds 11 to 45, the PPS even

reaches a faster decay rate of -0.6. The ATPPS and DAB decay rates do not change in this region. Similar to the Complete graph, the PPS and ATPPS curves stagnate again. Now with the difference that the PPS stagnates in an earlier round than the ATPPS. This can be seen again in the final region, where the decay rate of the PPS approaches zero. The DAB's lack of adaptability leads to slower convergence and less effective load balancing, as reflected in its consistently shallow decay rates. The MSE decreases from an initial value of 832 to approximately 480.47 for the DAB, while for the PPS and ATPPS algorithms, the MSE reaches values of 8.3×10^{-24} for the PPS and $\sim 6.5 \times 10^{-24}$ for the ATPPS.

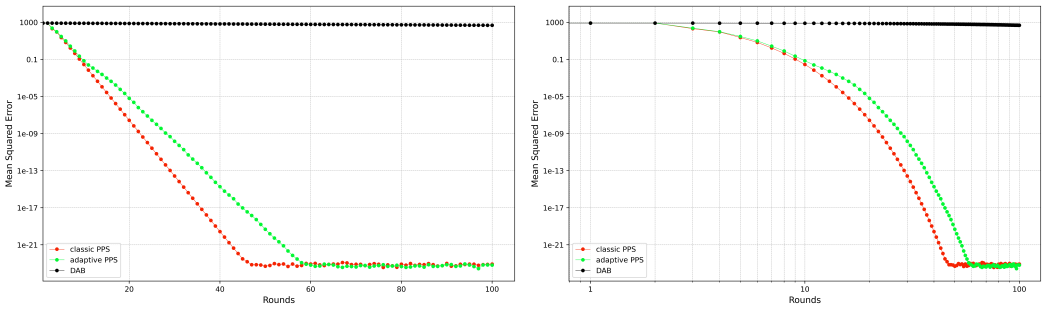

(a) **(b)**

Figure 20: Star graph: mean squared error per rounds (log-linear and log-log)

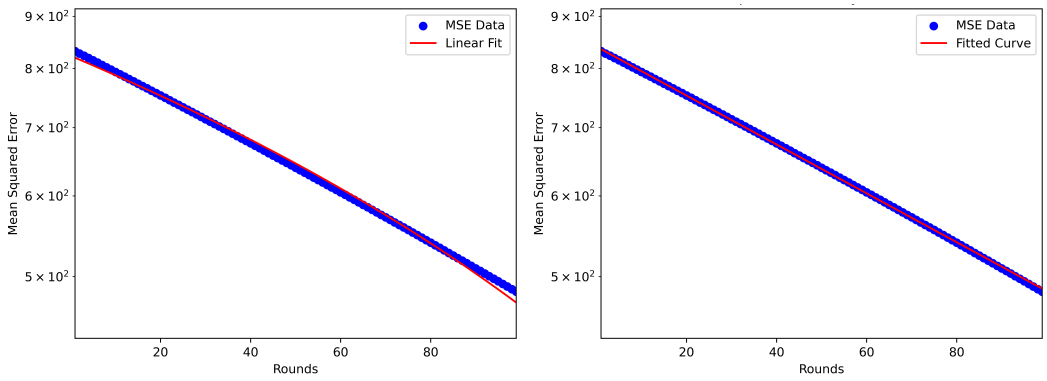

(a) **(b)**

Figure 21: Star graph - linear and exponential regression

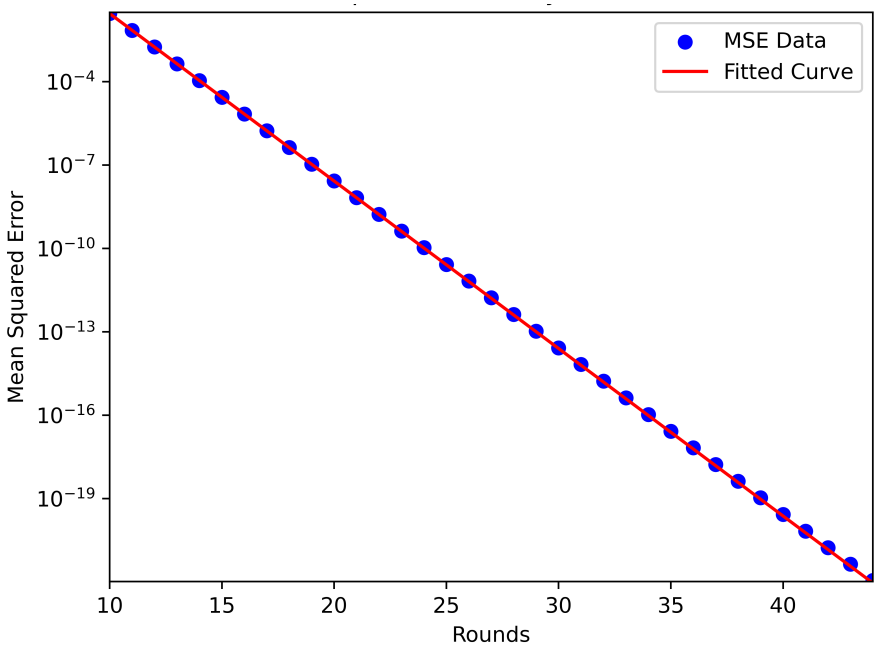

Figure 22: Star graph - exponential regression fit: PPS

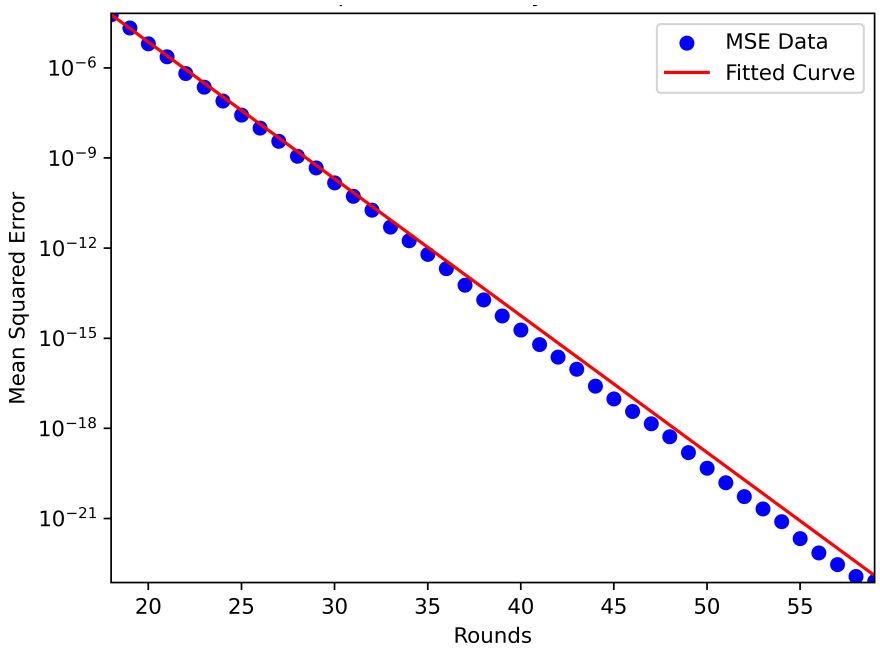

Figure 23: Star graph - exponential regression fit: ATPPS

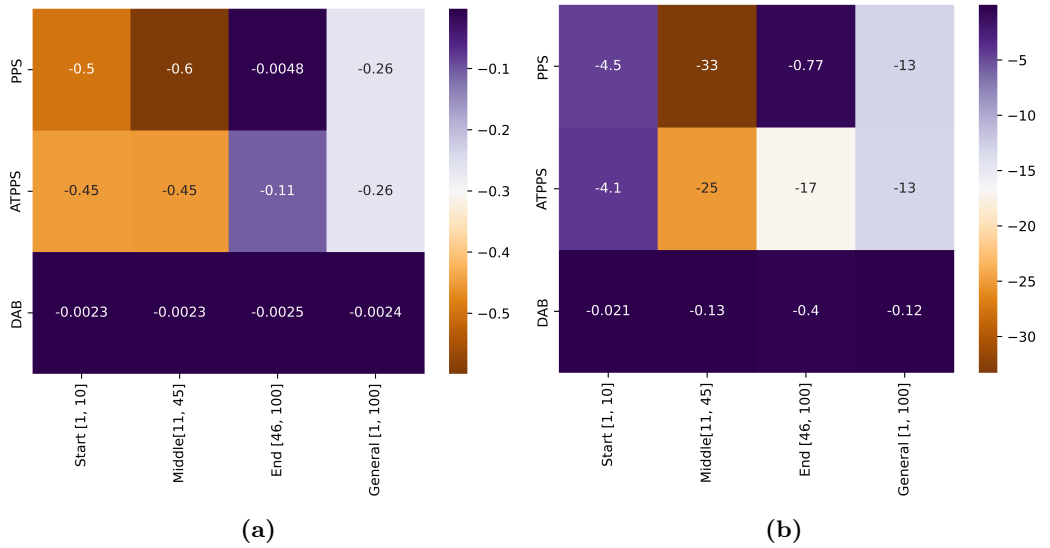

Figure 24: Star graph: heat map of slopes per region - log-linear and log-log

6.3 Ring Graph

The DAB curve in figure 25 shows the steepest decline in error in the first few rounds of the simulation. The slopes in figure 29, represent the exponents in the power-law relationship between the MSE and r. The slope of the first 10 rounds is -1.1 for the DAB curve compared to -0.94 ± 0.1 for each Push-Pull Sum based algorithm. The slopes decrease for all three algorithms to -0.53 ± 0.3 in the middle region and remain at these values for the end region. The near-overlap of PPS and ATPPS across the 100 rounds of simulation suggests that the adaptive mechanism provides limited additional benefit in a Ring graph, where selecting a random neighbor might already target an optimal load transfer partner. In a Ring topology, each node only interacts with its two immediate neighbors. The adaptive threshold mechanism relies on significant load differences between nodes to trigger transfers, but in a Ring graph, local load differences might not be significant enough to make the threshold mechanism advantageous. For the PPS, every node communicates with its neighbors in every round. This constant exchange ensures rapid propagation of

load. The adaptive threshold might reduce some of these exchanges; however, in a Ring graph, where the network diameter is large, reducing communication might delay convergence rather than improve it. The threshold mechanism could therefore counteract its own benefits and limit its advantage over the PPS. The DAB performs better in this scenario since it always interacts with the optimal partner to exchange loads. The benefit of randomness vanishes for a network topology where each node only has two neighbors, and a deterministic approach actually performs better.

The MSE data from each algorithm's simulations were fitted to a polynomial regression model of degree 4. The best-fit model for the DAB MSE data for rounds 10 to 60 follows the equation:

$$MSE_r = 1.72 \times 10^{-5} r^4 - 2.30 \times 10^{-3} r^3 + 0.19 r^2 - 5.99 r + 114.83 \tag{22}$$

as shown in figure 26. For small r the constant term dominates. As the time proceeds and r increases the higher-degree terms influence the behavior of the curve more and more. The MSE data of the PPS is fitted to a fourth-degree polynomial model:

$$MSE_r = 2.99 \times 10^{-5} r^4 - 0.5 \times 10^{-2} r^3 + 0.32 r^2 - 9.68 r + 166.30 \tag{23}$$

as shown in figure 27. The ATPPS MSE data is also fitted to a fourth-degree polynomial:

$$MSE_r = 3.04 \times 10^{-5} r^4 - 0.5 \times 10^{-2} r^3 + 0.32 r^2 - 9.64 r + 161.86 \tag{24}$$

as depicted in figure 28. The polynomial fit suggests that MSE reduction slows down over time.

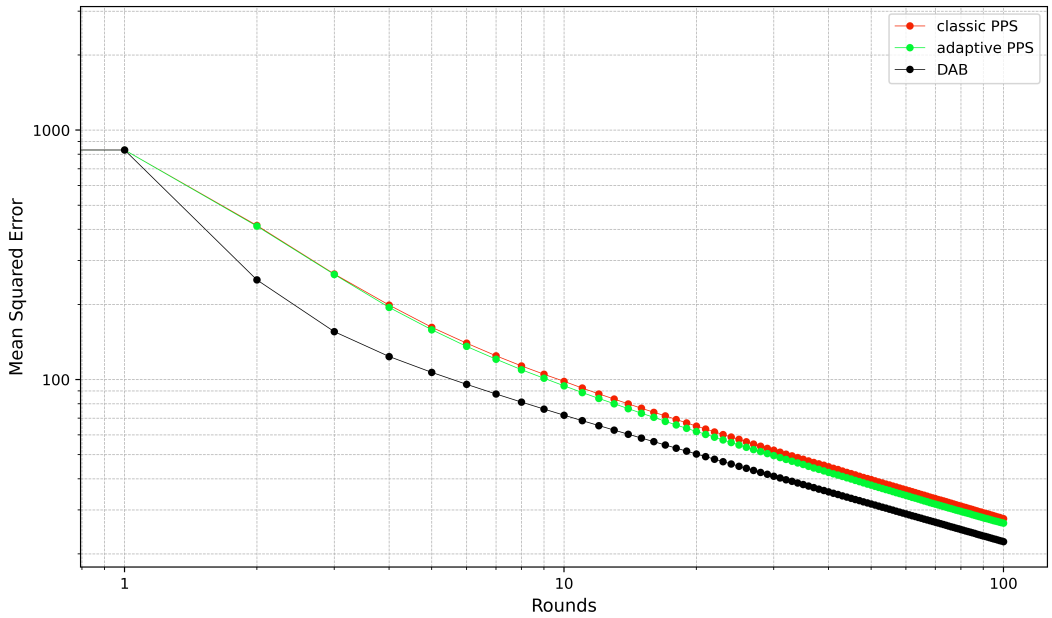

Figure 25: Ring graph: mean squared error per rounds (log-log)

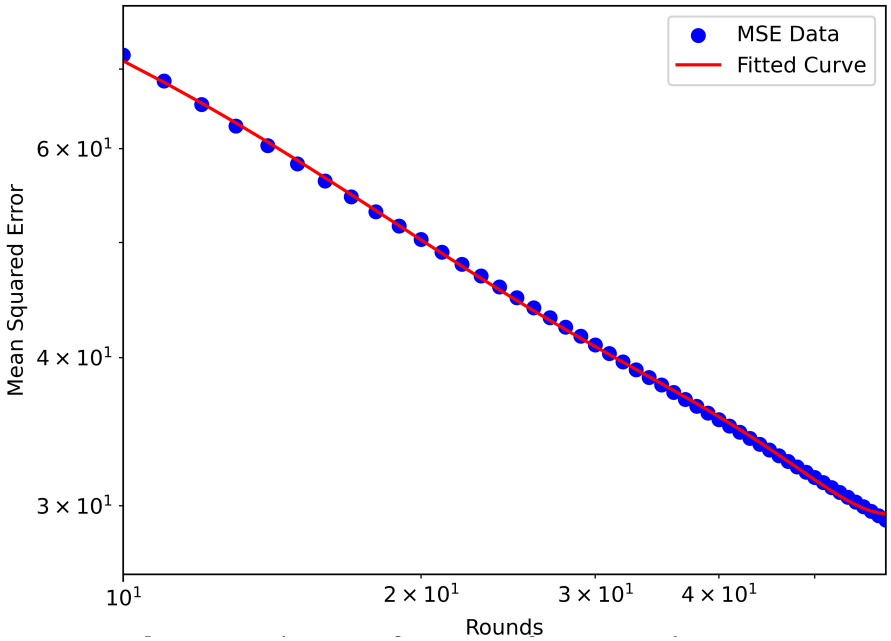

Figure 26: Ring graph - polynomial regression fit: DAB

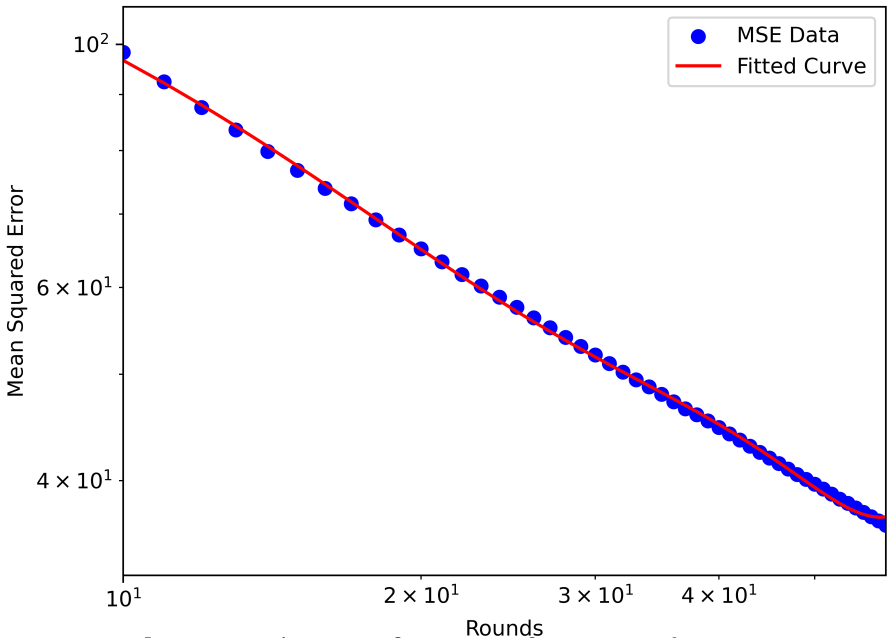

Figure 27: Ring graph - polynomial regression fit: PPS

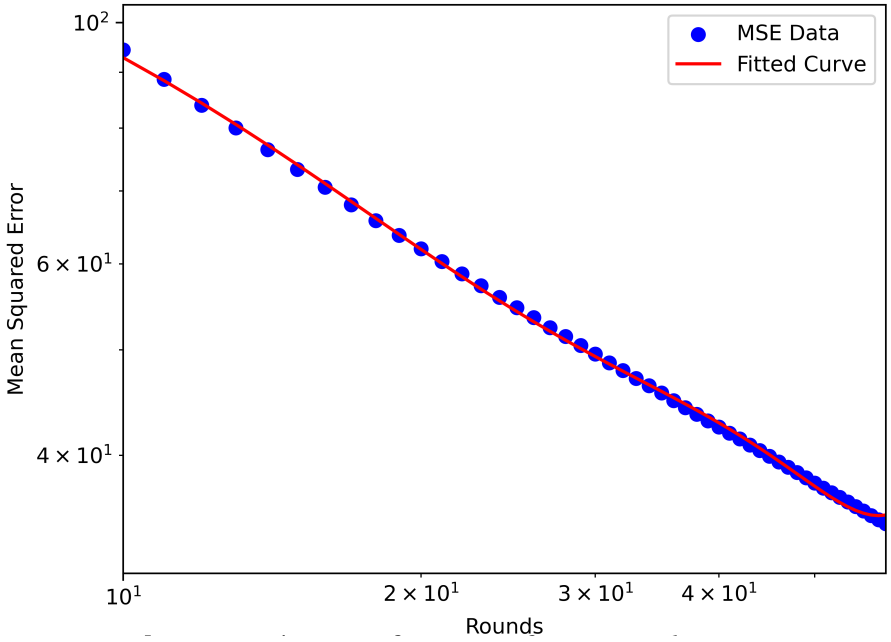

Figure 28: Ring graph - polynomial regression fit: ATPPS

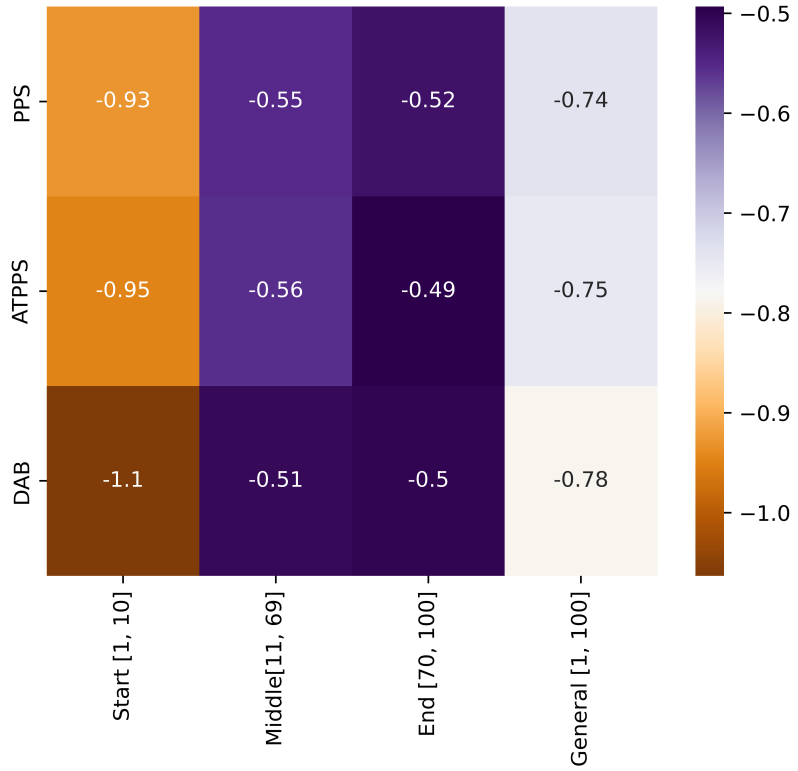

Figure 29: Ring graph: heat map of slopes per region - log-log

6.4 Torus Grid Graph

Figure 30 shows the MSE reduction over rounds on a Torus Grid graph, plotted on a log-log scale. The DAB curve has a slightly faster initial reduction compared to PPS' and ATPPS' curves in the beginning (rounds 1 to 7). The slope in this region is superior for the DAB algorithm with a value of -2.1 compared to approximately -1.5 for the Push-Pull Sum based algorithms (figure 34 - log-log). The PPS and ATPPS curves maintain nearly identical performances during the middle region (rounds 8 to 40), reducing MSE at a similar rate, with a slope of -1.2 for the PPS curve and -1.3 for the ATPPS curve. DAB shows a similar slope as the PPS. In the final region DAB scores the highest slope with a value of -2, followed by the ATPPS with a value of -1.7. The PPS achieves a slope of -1.4 in this region. This suggests that DAB and ATPPS adapt more efficiently to the graph's structure during intermediate rounds. PPS and ATPPS exhibit convergence, but they lag behind the DAB algorithm in reaching such low MSE values. Tori have more structured connectivity compared to a Star or Complete graph, allowing better distribution of loads via deterministic interactions. DAB's superior performance stems from it leveraging this regularity. The ATPPS algorithm achieves a balanced trade-off in this scenario. It outperforms the PPS approach, particularly in later rounds, where its adaptive mechanism prevents redundant load transfers and prioritizes exchanges that have a more significant impact on error reduction.

The uniform neighbourhood structure of Tori ensures that DAB's deterministic decisions (e.g., always choosing the minimal neighbor) are consistently effective across the graph. The algorithm does not suffer from suboptimal decisions introduced by probabilistic neighbor choices, which makes it well-suited to the topology. Both PPS and ATPPS protocols rely on randomly selecting a neighbor for load exchange. While this randomness is beneficial in irregular or dense graphs (e.g., Star or Complete graphs), it is less effective in structured topologies compared to the DAB, like a Torus Grid. The Push-Pull Sum-based algorithms do not always target the most unbalanced

areas. This means that load propagation can sometimes "stall" in certain regions, requiring more rounds to achieve global balance. The ATTPS draws its benefit over the PPS (especially in later rounds) by deciding which option of the available subset is the best. The discrepancy between the two load balancing algorithms widens in the last few rounds as trades between two nodes with higher load differences are more impactful once the network is already heavily balanced.

The fitted polynomial curve of degree 5 matches the MSE data for DAB effectively, capturing the non-linear dynamics during rounds 10 to 39 following the equation:

$$MSE_r = -1.35 \times 10^{-6} r^5 + 1.89 \times 10^{-4} r^4 - 0.01 r^3 + 0.30 r^2 - 4.6 r + 34.10 \quad (25)$$

as shown in figure 31 a). This suggests that in these rounds, the MSE reduction follows a complex pattern, as the loads propagate to different regions of the graph thanks to the wrap-around edges of the Tori. The higher degree captures these dynamics with more precision than simpler models, which is indicated by the R^2. In later rounds, the performance of the DAB can be captured by a polynomial curve of degree 3 with the equation:

$$MSE_r = -6.01 \times 10^{-06} r^3 + 1.66 \times 10^{-3} r^2 - 0.16 r + 6 \quad (26)$$

(figure 31 b)). At this stage, load balancing stabilizes, and the reduction in MSE becomes more linear or gradual. Thus, a lower-degree polynomial suffices to model the behavior in these later rounds. The curve behavior for the PPS and ATPPS are similar to that of the DAB curve expressed for rounds 10 to 39 by the equations:

$$MSE_r = -5.54 \times 10^{-6} r^5 + 7.65 \times 10^{-4} r^4 - 0.04 r^3 + 1.16 r^2 - 16.81 r + 112.86 \quad (27)$$

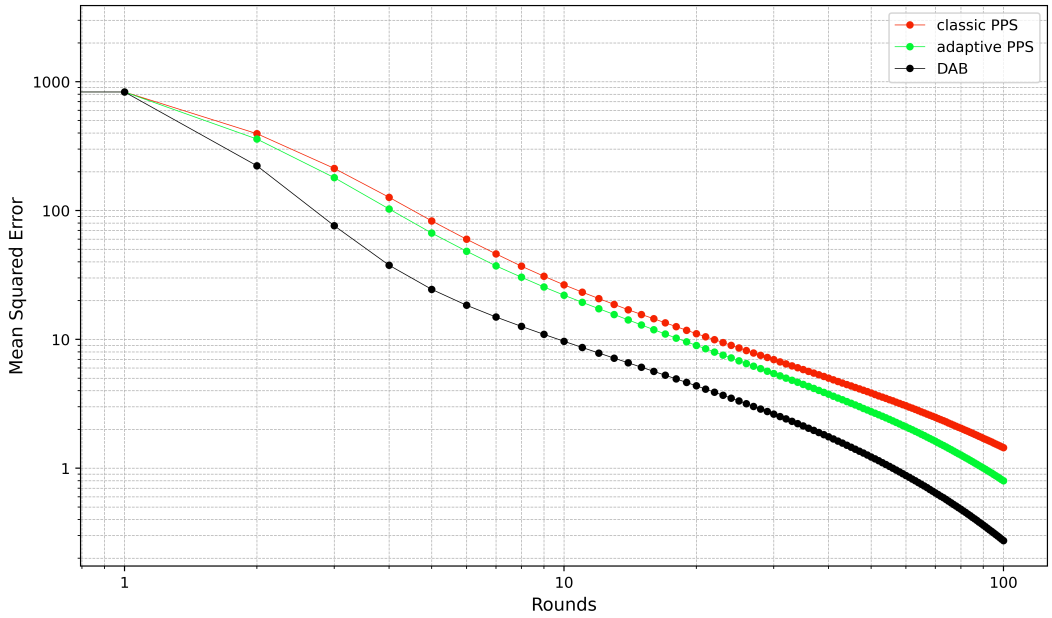

Figure 30: Torus Grid: mean squared error per rounds (log-log)

for the PPS (figure 32 a)) and:

$$MSE_r = -3.65 \times 10^{-6} r^5 + 5.16 \times 10^{-4} r^4 - 0.03 r^3 + 0.83 r^2 - 12.52 r + 88.16 \quad (28)$$

for the ATPPS (figure 33 a)). The equations that describe the behavior of the two Push-Pull Sum based algorithms are fitted for rounds 40 to 100 for the PPS:

$$MSE_r = -1.15 \times 10^{-5} r^3 + 3.205 \times 10^{-3} r^2 - 0.33 r + 13.72 \quad (29)$$

(figure 32 b)) and for the ATPPS is:

$$MSE_r = -9.99 \times 10^{-6} r^3 + 2.80 \times 10^{-3} r^2 - 0.28 r + 11.29 \quad (30)$$

(figure 33 b)).

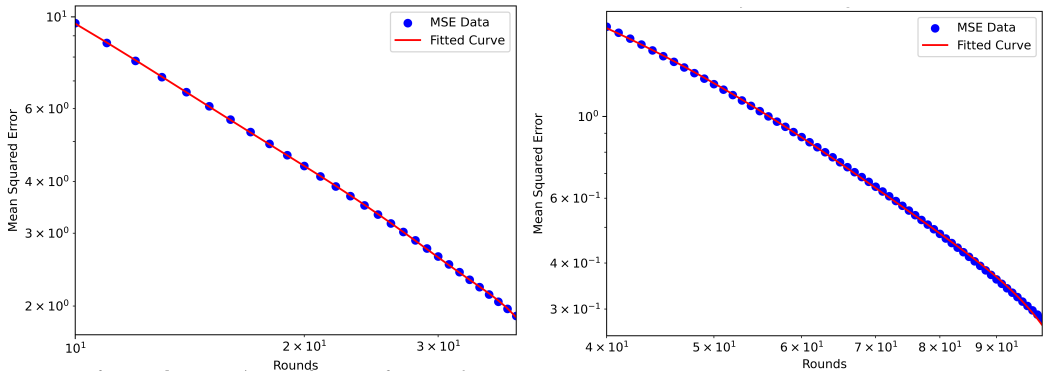

(a) (b)

Figure 31: Torus Grid - polynomial regression fit: DAB; rounds 10-39 and 40-100

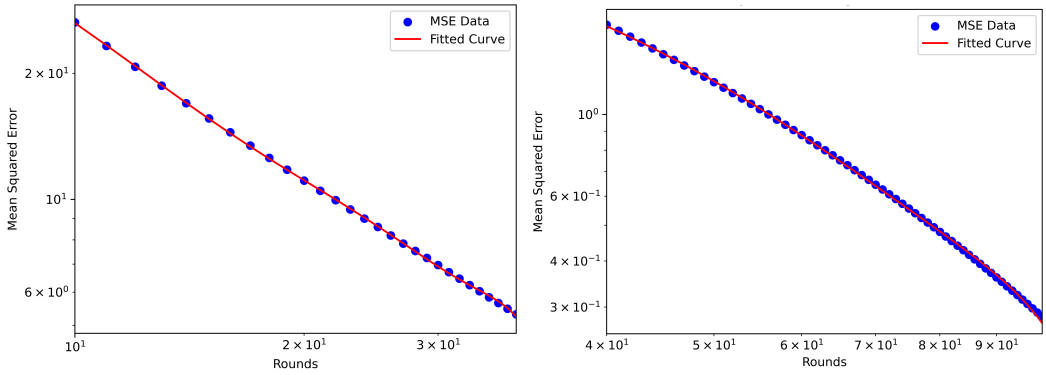

(a) (b)

Figure 32: Torus Grid - polynomial regression fit: PPS; rounds 10-39 and 40-100

6.5 Lollipop Graph

6.5.1 (512, 512) Lollipop Graph

Figure 35 displays the three curves of the load balancing algorithms. The ATPPS slightly outperforms the PPS, while the DAB algorithm underperforms compared to both Push-Pull Sum-based methods in reducing the error. The superior performance of PPS and ATPPS compared to DAB in the Lollipop graph can be explained by the structure of the graph and the fundamental differences in how these algorithms operate. The clique region is characterized by high connectivity and enables rapid

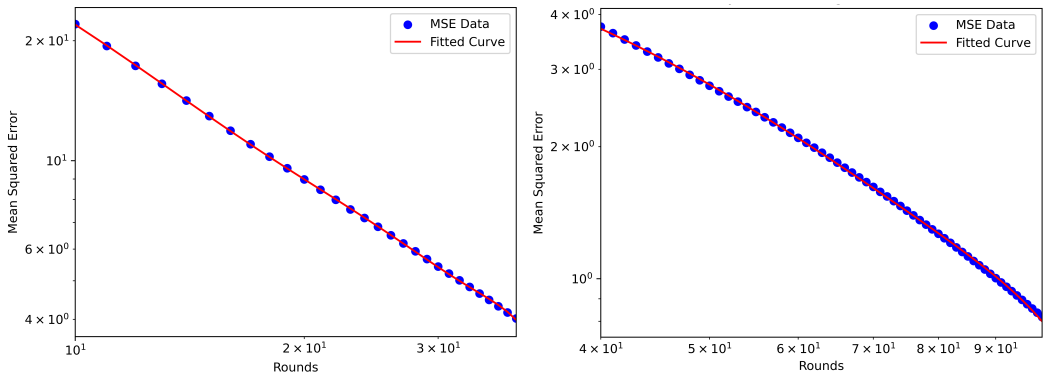

Figure 33: Torus Grid - polynomial regression fit: ATPPS; rounds 10-39 and 40-100

local balancing for the Push-Pull Sum based algorithms. While the path region with limited connectivity slows down information propagation and balancing for the Push-Pull Sum-based algorithms and favors the deterministic DAB. The initial discrepancy in the first 10 rounds arises due to the potentially rapid error reduction achieved by PPS within the clique. The DAB struggles to perform well for cliques, as observed in section 6.1. DAB performs rather well in the Path graph which in theory is similar to the Ring graph without the edge connecting the first and last nodes as described in section 6.3. It prioritizes nodes with the least load, which can lead to inefficient propagation along the clique. DAB does not exploit the random spreading mechanism of the Push-Pull Sum-based algorithms. In the initial phase, PPS rapidly reduces the MSE, demonstrating strong initial convergence. The Push-Pull Sum-based algorithms achieve a steep downward slope with value -1.3 between rounds 1 and 7, while the DAB achieves a value of -0.34 (figure 39). In the mid-to-late phase, the slope flattens for both Push-Pull Sum-based algorithms, indicating slower convergence. This is evident from the slope values dropping to as low as -0.56 for PPS and -0.57 for ATPPS. In this phase, the path section of the Lollipop graph dominates the residual imbalances. The ATPPS achieves nearly identical behavior to the PPS in the early rounds, as it starts with similar strategies where the threshold is relatively easy to surpass as the load differences in the network

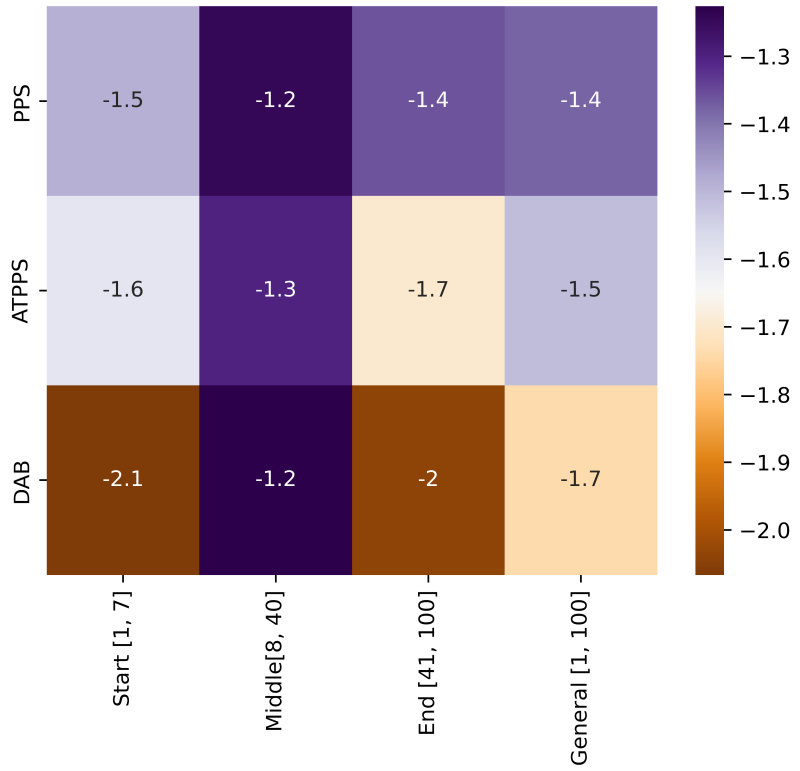

Figure 34: Torus Grid: heat map of slopes per region - log-log

are still very high. ATPPS outperforms the PPS slightly in the later rounds due to its ability to dynamically adjust its balancing strategy based on the current state of load imbalances. This allows it to better address residual imbalances in the path section of the Lollipop graph as showcased in section 6.3.

The MSE data for the DAB algorithm is best described by a polynomial of degree 3, following the equation:

$$MSE_r = -5.89 \times 10^{-5} r^3 + 0.03 r^2 - 5.68 r + 459.42 \tag{31}$$

as shown in figure 36. The MSE trends for the PPS and ATPPS algorithms are better captured by polynomials of degree 4. The best-fit equation for the PPS model is:

$$MSE_r = 8.44 \times 10^{-7} r^4 - 2.52 \times 10^{-4} r^3 - 0.03 r^2 - 1.64 r + 56.68 \tag{32}$$

(figure 37) and the ATPPS model fit follows the equation:

$$MSE_r = 8.69 \times 10^{-7} r^4 - 2.56 \times 10^{-4} r^3 + 0.03 r^2 - 1.62 r + 54.48 \tag{33}$$

(figure 38).

To analyze the impact of the path size and clique size on the simulation results, additional simulations were conducted with varying proportions of nodes assigned to each region. In subsection 6.5.2, the number of nodes assigned to the clique is reduced to 128, which is one-fourth of the previous value of 512. Consequently, the path section now consists of 896 nodes. The total network size remains unchanged. This adjustment allows us to observe how a more dominant path section influences the load balancing behavior of the different algorithms. Similarly, in subsection 6.5.3, the simulations are performed with a reduced path size, assigning 896 nodes to the clique and only 128 nodes to the path. This configuration provides insight into how a more densely connected clique affects the overall performance of the algorithms.

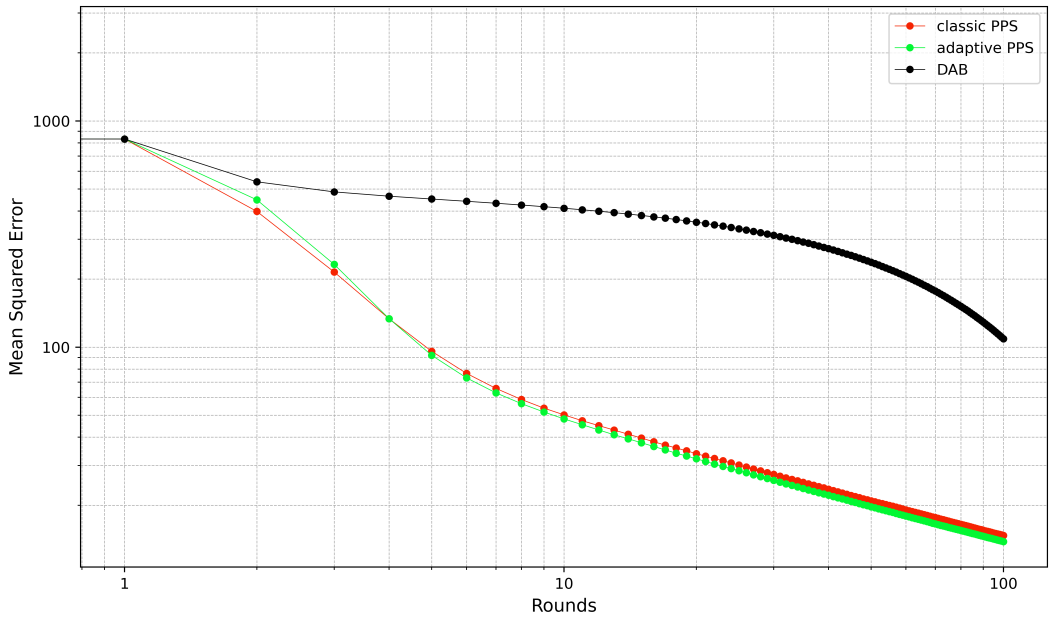

Figure 35: (512, 512)-Lollipop graph: mean squared error per rounds (log-log)

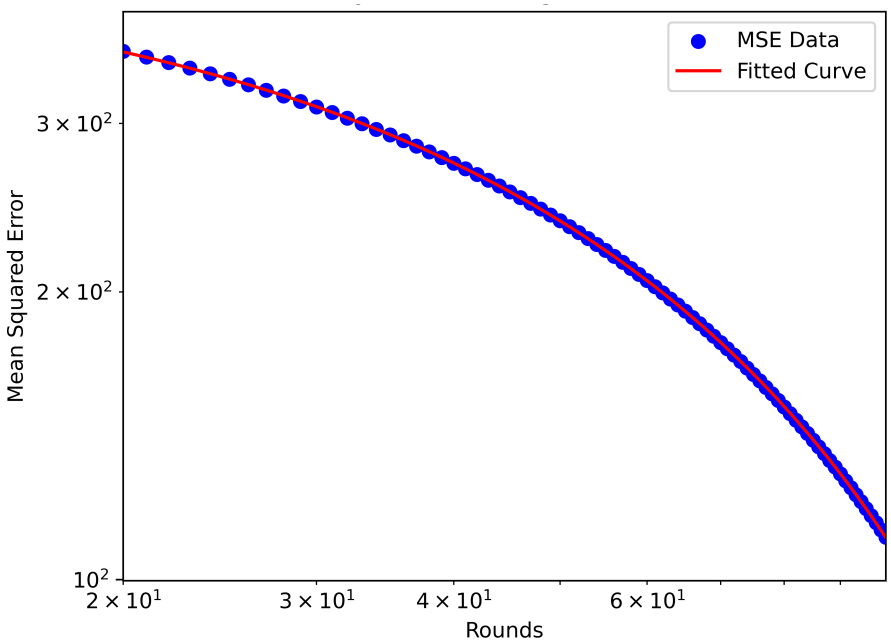

Figure 36: (512, 512)-Lollipop graph - polynomial regression fit: DAB

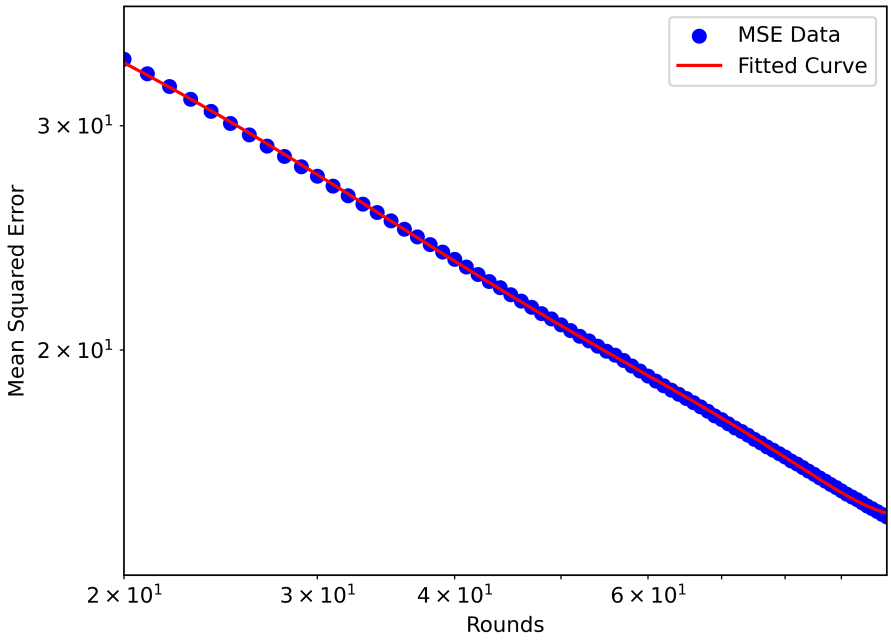

Figure 37: (512, 512)-Lollipop graph - polynomial regression fit: PPS

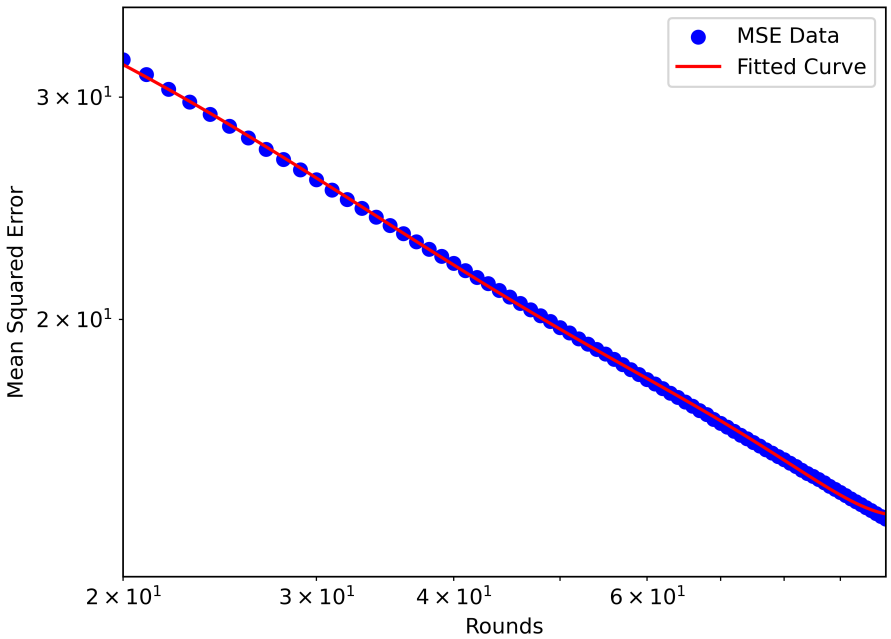

Figure 38: (512, 512)-Lollipop graph - polynomial regression fit: ATPPS

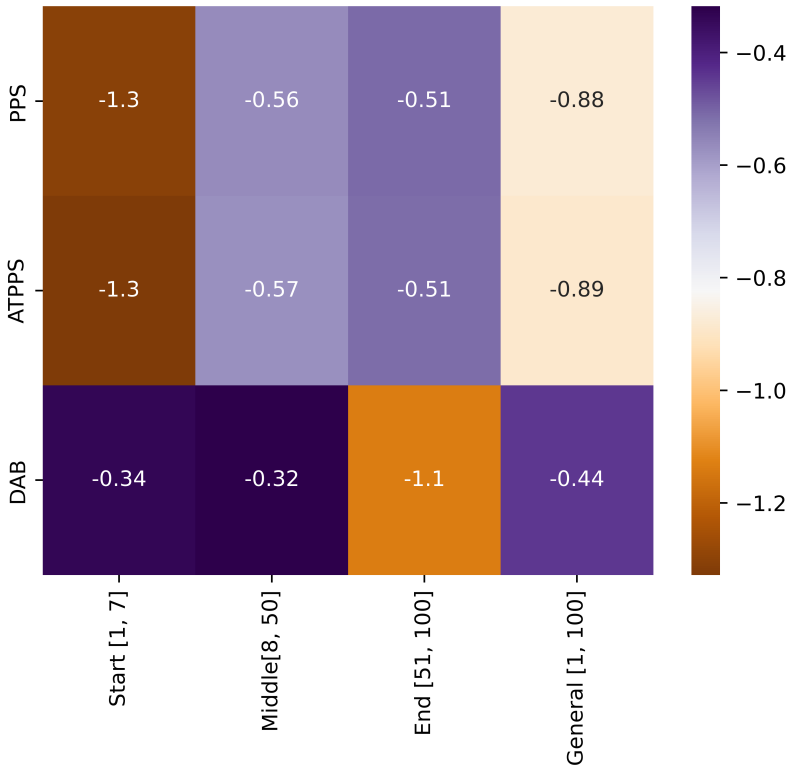

Figure 39: (512, 512)-Lollipop graph: heat map of slopes per region - log-log

6.5.2 (128, 896) Lollipop Graph

In the initial phase (the first 7 rounds) PPS and ATPPS start with a steep decline in MSE, both with a slope of -1.2, as shown in figure 44. DAB, on the other hand, demonstrates a slightly slower initial convergence, with a slope of -0.86. Compared to the previous experiment, where the path and clique sizes were equal, DAB's performance in the initial rounds has improved. The slope in this region in the previous experiment was -0.34 and improved to -0.86, which indicates a faster initial error reduction. In the middle region, rounds 8 to 50, the ATPPS shows a performance close to that of the PPS where both curves maintain a consistently steep slope. In the middle region, the PPS manages to increase its performance again slightly, recognisable by the fact that the slope has fallen by 0.1. The ATPPS manages to close the MSE discrepancy to the PPS in the end region. In this region, the ATPPS emits the largest drop in MSE. In the end phase the DAB shows a slightly shallower decline (-0.78) in MSE compared to earlier rounds. This could be attributed to the fact that once most of the load has propagated through the path, the balancing process along the clique slows. Both Push-Pull Sum variants continue to outperform DAB, achieving lower MSE values in fewer rounds due to their efficient clique-based load redistribution. Interestingly, PPS and ATPPS exhibit a slight divergence between rounds 10 and 90, before finally intersecting (or nearly so) around round 100. The PPS and ATPPS MSE data are very close to each other in round 100, suggesting that the ATPPS does not lead to an improved load balancing behaviour.

The MSE data of all three load balancing algorithms were fitted to polynomial regression models. The MSE data for DAB and ATPPS were best approximated by polynomials of degree 4, while the PPS MSE data exhibited slightly more complex behavior, following a polynomial of degree 5. The fitted model for the DAB MSE

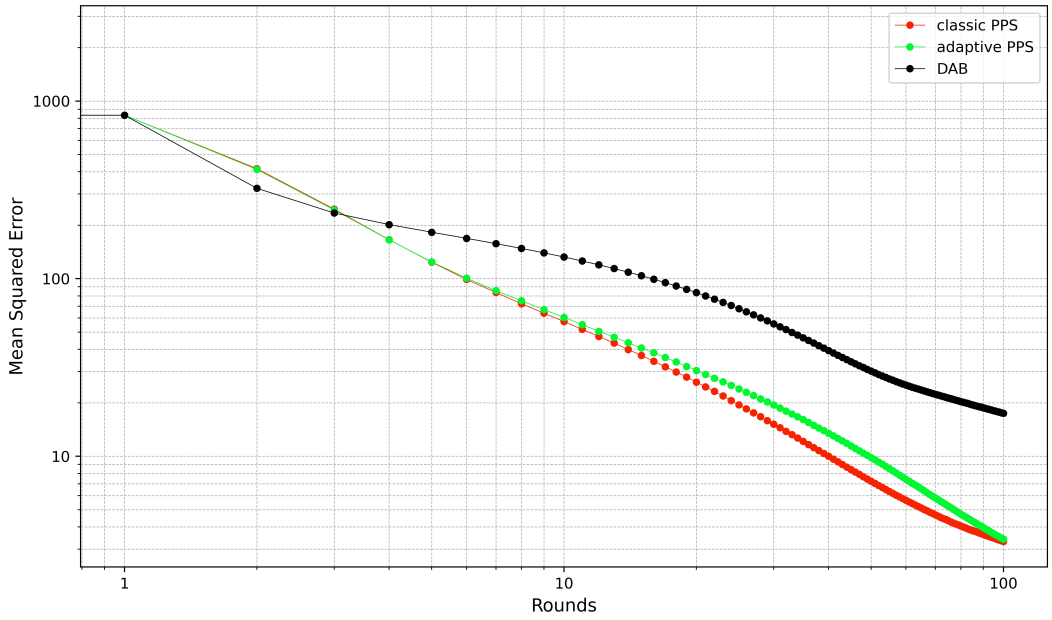

Figure 40: (128, 896)-Lollipop graph: mean squared error per rounds (log-log)

data follows the equation:

$$MSE_r = 3.46 \times 10^{-6} r^4 - 1.12 \times 10^{-3} r^3 + 0.14 r^2 - 7.69 r + 190.78 \tag{34}$$

(figure 41). For ATPPS, the polynomial fit is given by

$$MSE_r = 1.59 \times 10^{-6} r^4 - 4.74 \times 10^{-4} r^3 + 0.054 r^2 - 2.94 r + 70.59 \tag{35}$$

(figure 42). The PPS MSE data, which required a higher-degree polynomial (degree 5), follows the equation.

$$MSE_r = -3.72 \times 10^{-8} r^5 + 1.31 \times 10^{-5} r^4 - 1.85 \times 10^{-3} r^3 + 0.13 r^2 - 4.96 r + 84.91 \tag{36}$$

(figure 43).

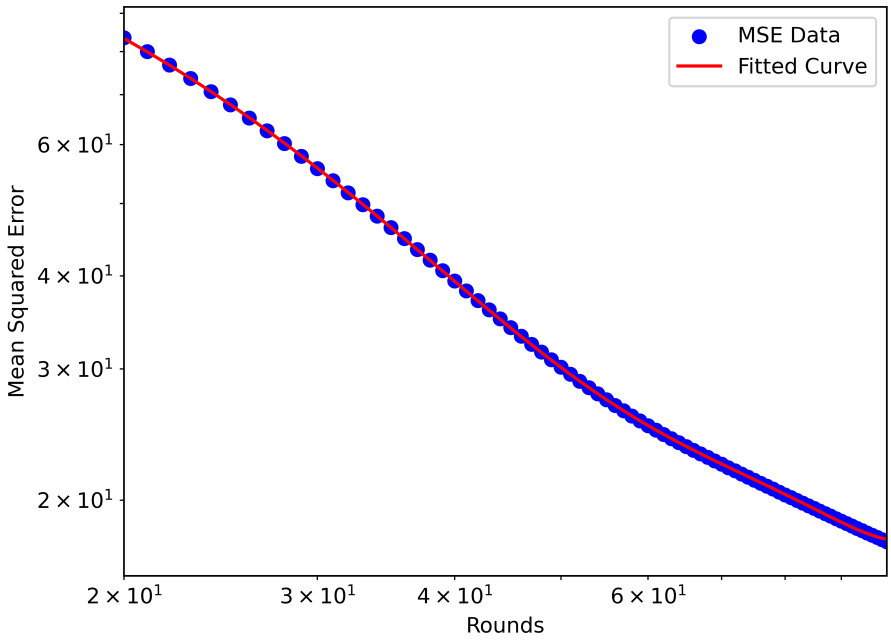

Figure 41: (128, 896)-Lollipop graph - polynomial regression fit: DAB

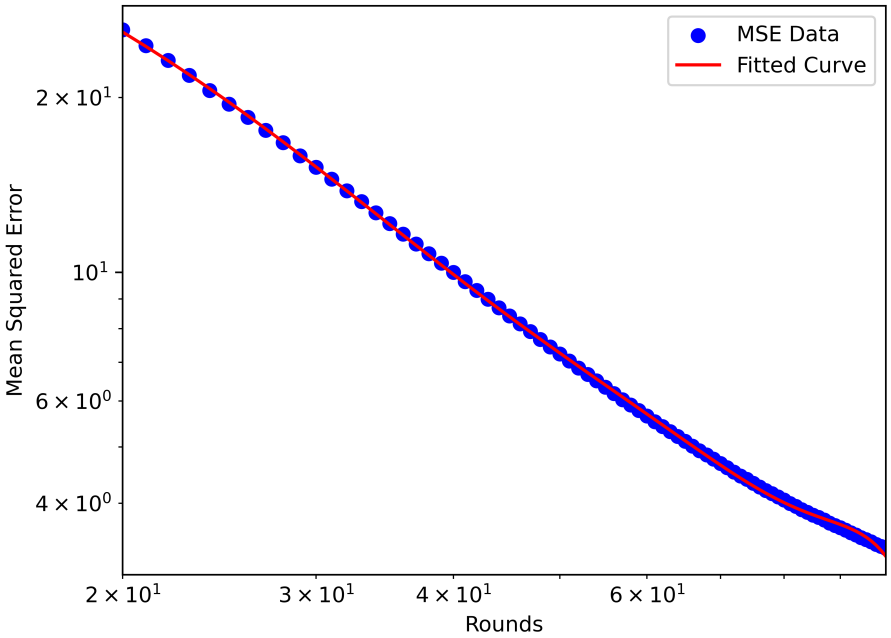

Figure 42: (128, 896)-Lollipop graph - polynomial regression fit: PPS

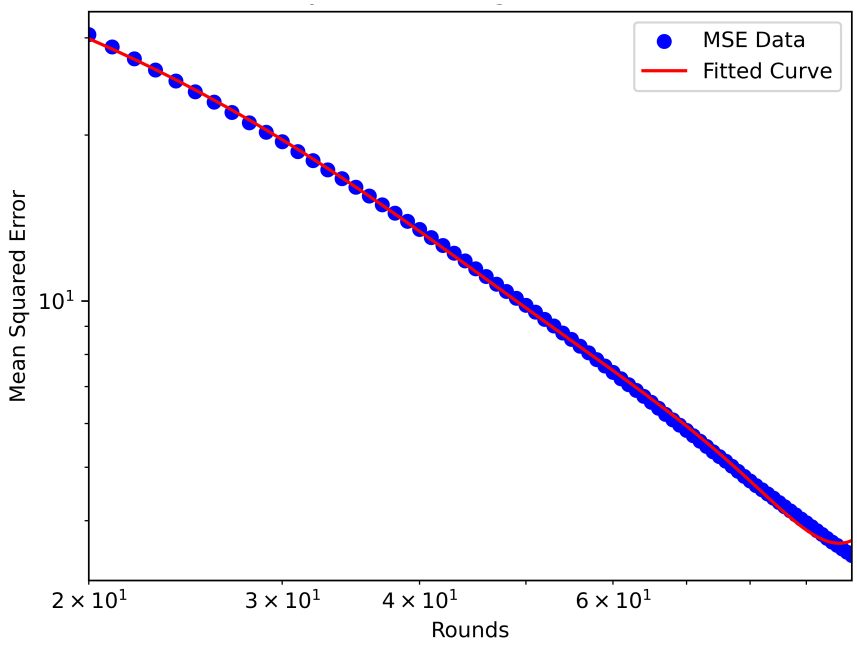

Figure 43: (128, 896)-Lollipop graph - polynomial regression fit: ATPPS

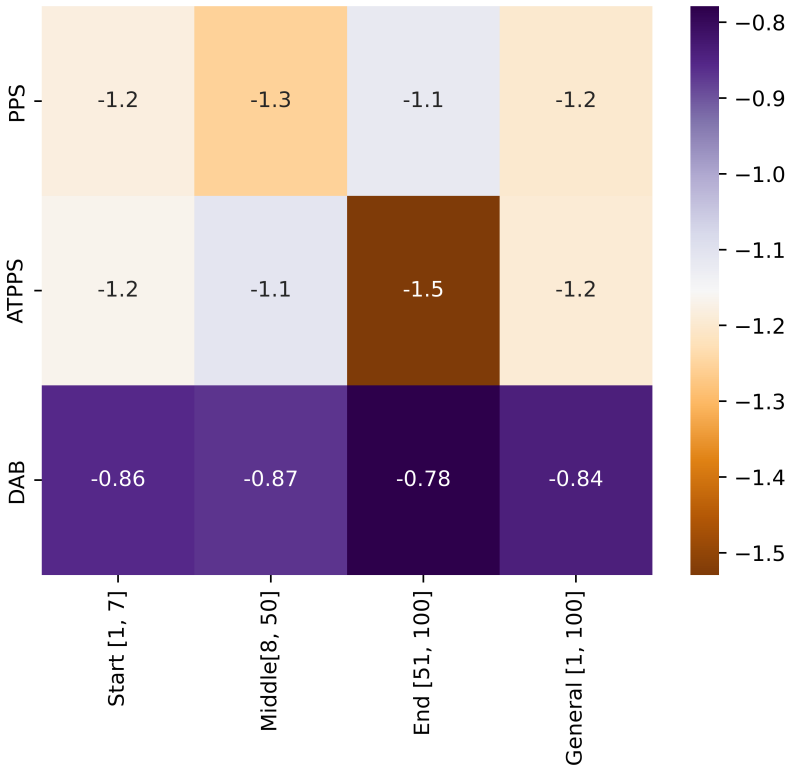

Figure 44: (128, 896)-Lollipop graph: heat map of slopes per region - log-log

6.5.3 (896, 128) Lollipop Graph

As more nodes are assigned to the clique and fewer to the path in the (896, 128)-Lollipop graph compared to the (512, 512)-Lollipop graph, the performance gap between the Push-Pull Sum based algorithms and the DAB becomes more pronounced, as shown in figure 45. This is also reflected in the log-log slopes. In the start region, the Push-Pull Sum based algorithms balance the network more quickly in the (896, 128)-Lollipop graph, achieving slopes of -2, compared to -1.3 in the (512, 512)-Lollipop graph (figure 49). In the middle and end region, the slopes are almost quartered compared to the start region. The DAB only achieves consistently low slopes: -0.08 in the start region, -0.1 in the middle region and -0.11 in the end region. The overall MSE is also lower for the (896, 128)-Lollipop graph, with the ATPPS reducing the error to 3.27 and the PPS to 3.59. In contrast, the MSE values for the (512, 512)-Lollipop graph are higher after 100 rounds, where ATPPS achieved a value of 13.83 and the PPS achieved a value of 14.71. Despite this, no significant advantage of the ATPPS over the PPS is observed. The DAB, however, struggles to reduce the error, with a substantial difference in MSE values after 100 rounds. In the (512, 512)-Lollipop graph, the DAB reaches an MSE of 108.90, while in the (896, 128)-Lollipop graph, the MSE increases to 542.09—almost five times higher.

The best-fit polynomials for the MSE data of the load balancing algorithms are of degree 3 for the DAB and degree 4 for the Push-Pull Sum-based algorithms. The polynomial for the DAB MSE data is expressed as

$$MSE_r = -1.936 \times 10^{-4} r^3 + 0.05 r^2 - 5.33 r + 745.95 \tag{37}$$

(figure 46). For the PPS, the polynomial is:

$$MSE_r = 2.00 \times 10^{-7} r^4 - 6.01 \times 10^{-5} r^3 + 6.95 \times 10^{-3} r^2 - 0.39 r + 13.44 \tag{38}$$

(figure 47) and for the ATPPS, is:

$$MSE_r = 2.28 \times 10^{-7} r^4 - 6.77 \times 10^{-5} r^3 + 7.68 \times 10^{-3} r^2 - 0.42r + 13.62 \quad (39)$$

(figure 48).

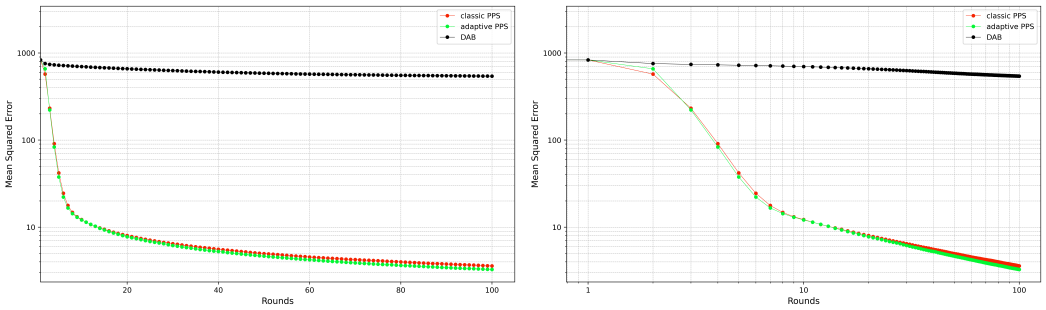

(a) **(b)**

Figure 45: (896, 128)-Lollipop graph: mean squared error per rounds (log-linear and log-log)

6.6 Ring of Cliques

6.6.1 32x32 Ring of Cliques

In the early rounds, PPS and ATPPS exhibit the fastest MSE reduction, as shown by a very steep downward trend between rounds 1 and 5 in figure 50 b). Both Push-Pull Sum-based approaches demonstrate faster convergence rates compared to DAB. The initial steep downward slope of around -1.8 for each Push-Pull Sum-based algorithm, as depicted in figure 54, within the first 5 rounds is due to the unbalanced state of each clique. These algorithms perform better than DAB in Complete graph scenarios. During this phase, while the cliques remain unbalanced, the Push-Pull Sum-based algorithms achieve rapid convergence. Once the cliques start to balance, round by round, DAB catches up, especially between rounds 6 and 40, where the slopes are -2.1 for the DAB compared to approximately -0.5 for the Push-Pull

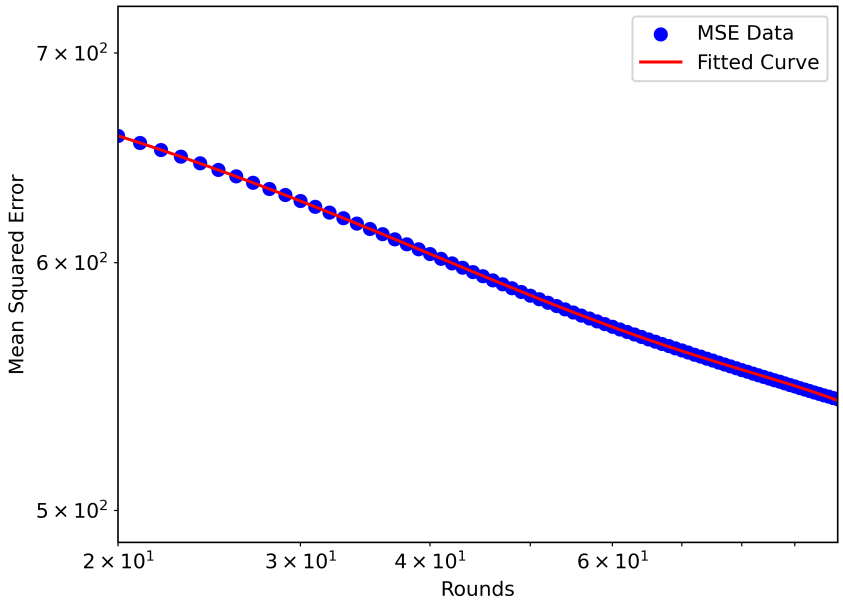

Figure 46: (896, 128)-Lollipop graph - polynomial regression fit: DAB

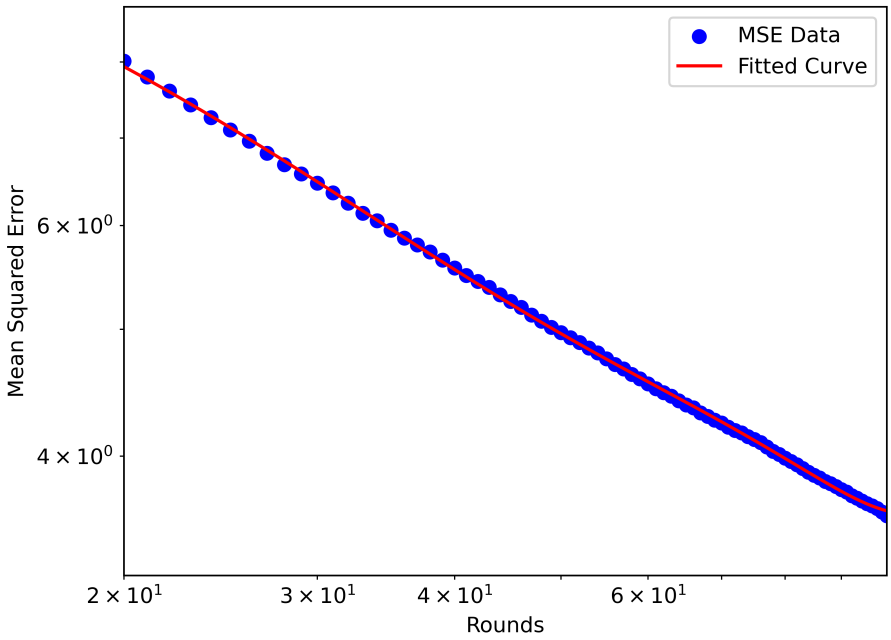

Figure 47: (896, 128)-Lollipop graph - polynomial regression fit: PPS

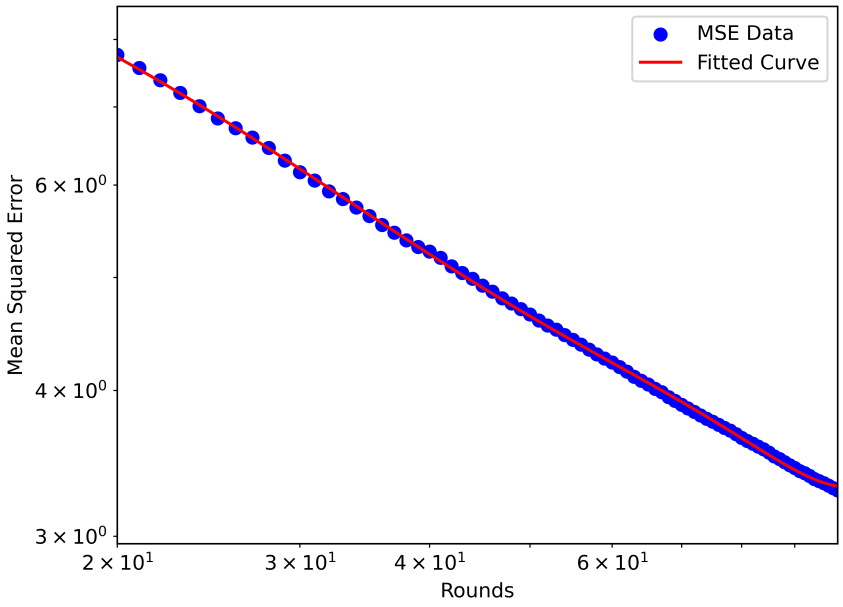

Figure 48: (896, 128)-Lollipop graph - polynomial regression fit: ATPPS

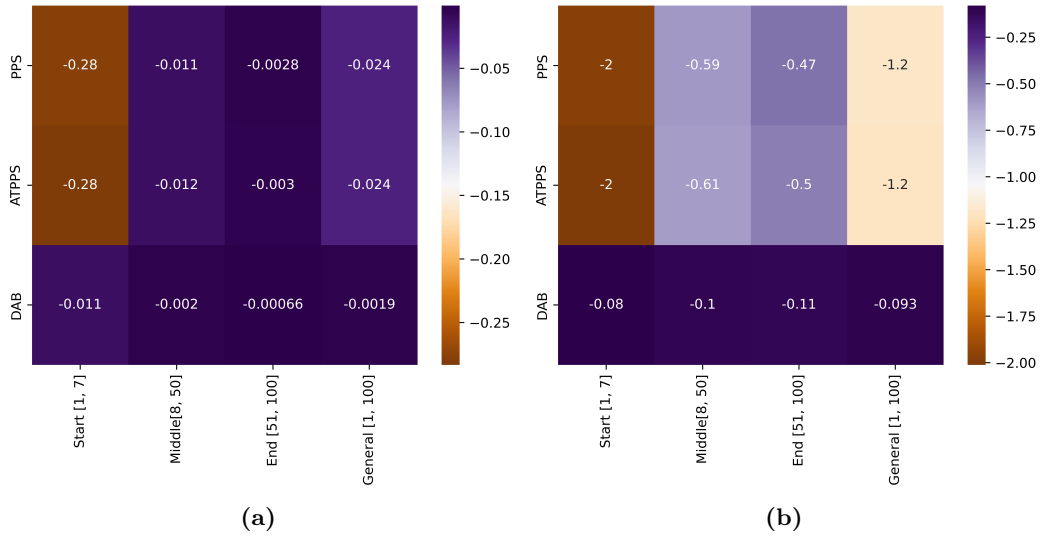

Figure 49: (896, 128)-Lollipop graph: heat map of slopes per region - log-linear and log-log

Sum-based algorithms. Nodes within cliques tend to converge quickly internally due to their dense interconnections for the Push-Pull Sum-based algorithms. However, load balancing between cliques, especially when the nodes select random neighbors,

is slower, creating bottlenecks for global convergence (this is especially the case for the PPS, whose curve starts to stagnate between round 10 and 100). Thanks to the deterministic load balancing strategies, the bridging nodes choose nodes outside of their cliques once the load is balanced within the clique and spread the load to other cliques. The ATPPS algorithm achieves better results compared to the PPS since it has a similar mechanism in this scenario like the DAB, prioritizing communication between cliques (where differences in loads are more significant) over redundant communication within cliques (where loads are already close to balanced). This is reflected in the behavior of the curve after round 10. Again, the ATPPS acts as a compromise solution between the PPS and the DAB, achieving results close to those of the DAB algorithm. Overall, at round 100 the DAB achieved an MSE of approximately 6.55, the PPS an MSE of 19.80, and the ATPPS an MSE of 8.42.

The polynomial fit for the DAB algorithm is expressed as

$$MSE_r = 1.04 \times 10^{-6} r^4 - 2.941 \times 10^{-4} r^3 + 0.03 r^2 - 1.66 r + 45.30 \tag{40}$$

(figure 51), which models the MSE data as a function of rounds with a fourth-degree polynomial. For the PPS algorithm, the MSE data from rounds 20 to 100 is fitted to a linear regression model

$$MSE_r = -0.05 r + 24.70 \tag{41}$$

(figure 52). The negative slope indicates a consistent reduction in MSE with each round in this region, though the value -0.05 is relatively small. This suggests that the PPS algorithm achieves slow and steady progress toward a balanced network. The linear fit suggests that PPS achieves only gradual improvement in balancing the load in the Ring of Cliques topology. The reason for that is that PPS focuses on a push-pull mechanism that is, relying on random neighbor interactions. In the Ring of Cliques, inter-clique connections are sparse, and PPS lacks a mechanism to prioritize balancing between these sparsely connected regions. As a result, its performance

is bottlenecked by the topology. The linear regression model highlights a uniform rate of error reduction over the rounds, with no acceleration observed, unlike other approaches like DAB. The logarithmic model for the ATPPS algorithm is given by

$$\log(MSE_r) = -7.59 \log(r) + 43.26 \tag{42}$$

(figure 53). By exponentiating this equation, the relationship between MSE and the number of rounds can be written as

$$MSE_r = 10^{43.26} * r - 7.59. \tag{43}$$

The steep negative slope of -7.59 in the log-log fit indicates a rapid decrease in MSE as the number of rounds increases. This suggests that ATPPS achieves exponentially faster convergence compared to PPS, particularly in the early rounds of load balancing.

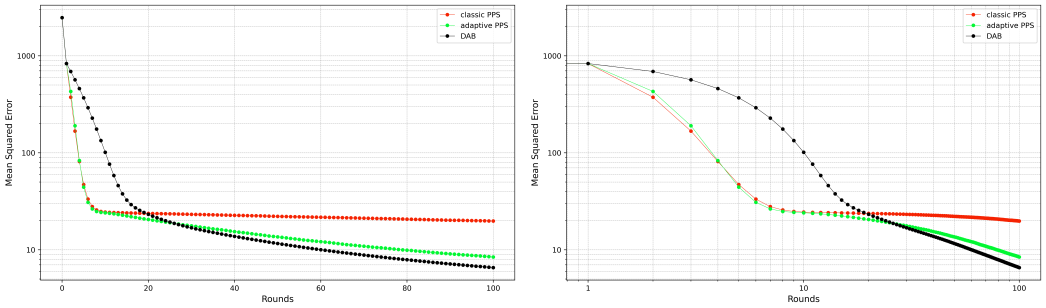

(a) **(b)**

Figure 50: (32×32)-Ring of Cliques: mean squared error per rounds (log-linear and log-log)

In the following experiments, the structure of the Ring of Cliques is reorganized. The number of cliques is increased from 2^5 to 2^7 in subsection 6.6.2, which results in a decrease in the size of each clique to 2^3. Subsection 6.6.3 covers the experiment where the clique size is increased, while the number of cliques is decreased by the same magnitude.

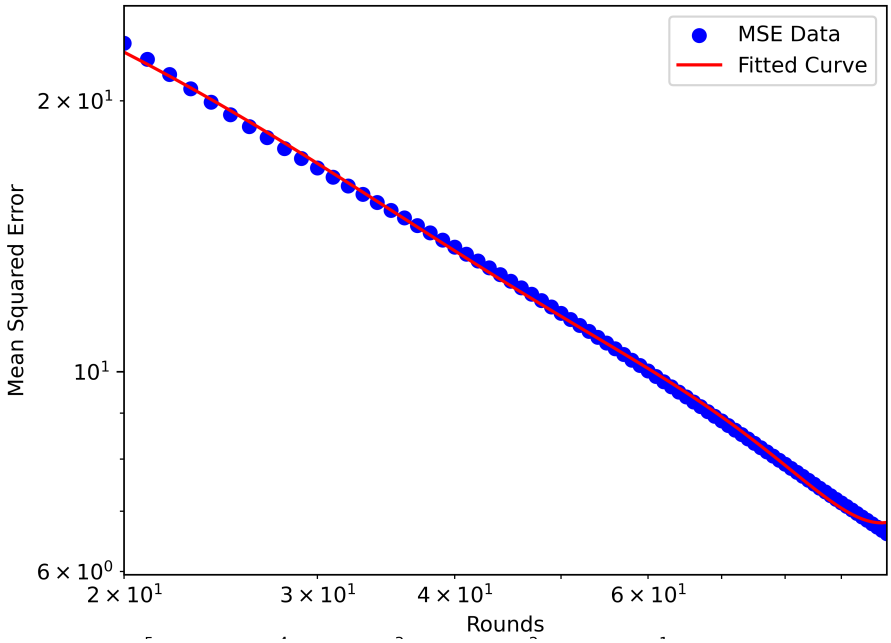

Figure 51: (32×32)-Ring of Cliques - polynomial regression fit: DAB

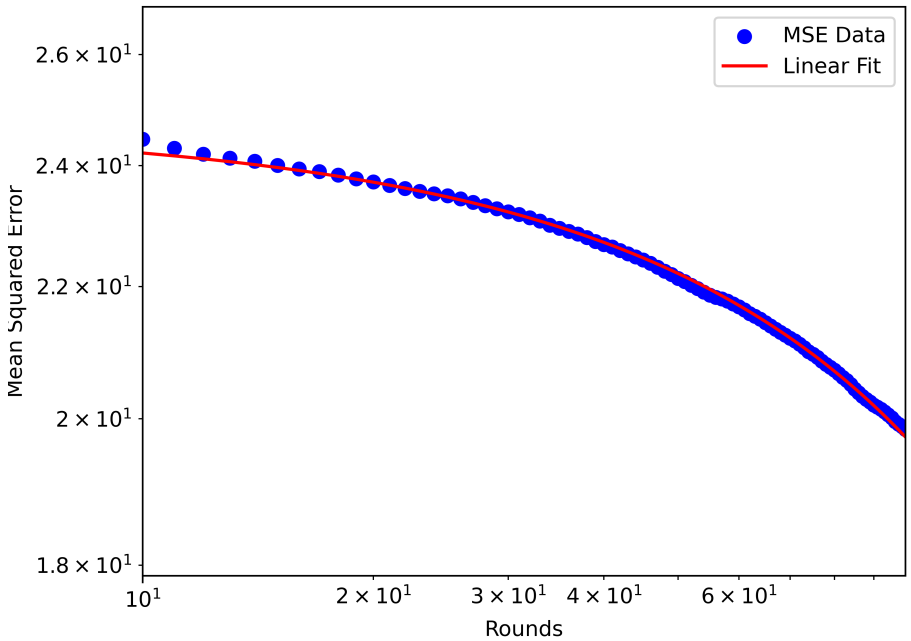

Figure 52: (32×32)-Ring of Cliques - linear regression fit: PPS

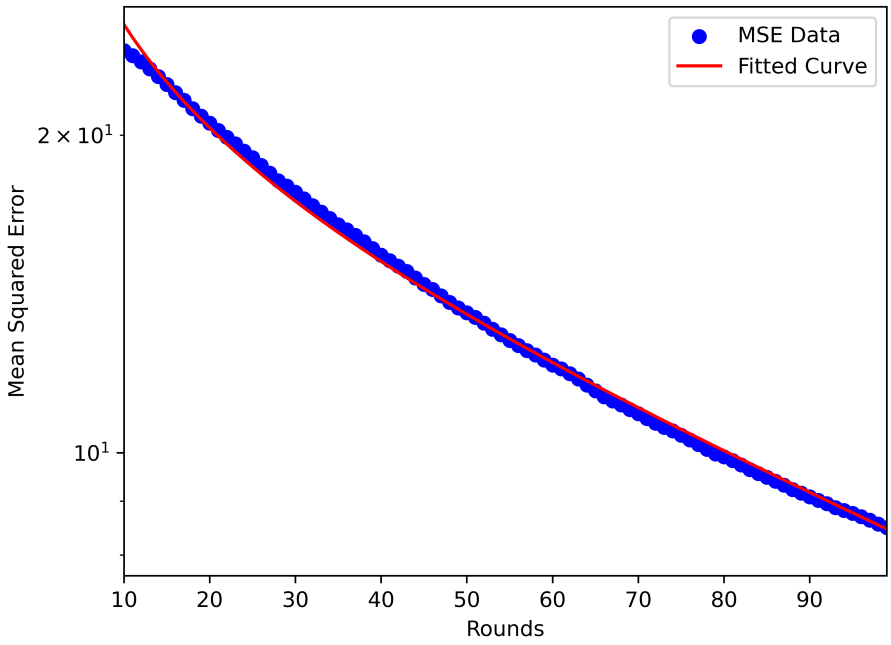

Figure 53: (32×32)-Ring of Cliques - logarithmic regression fit: ATPPS

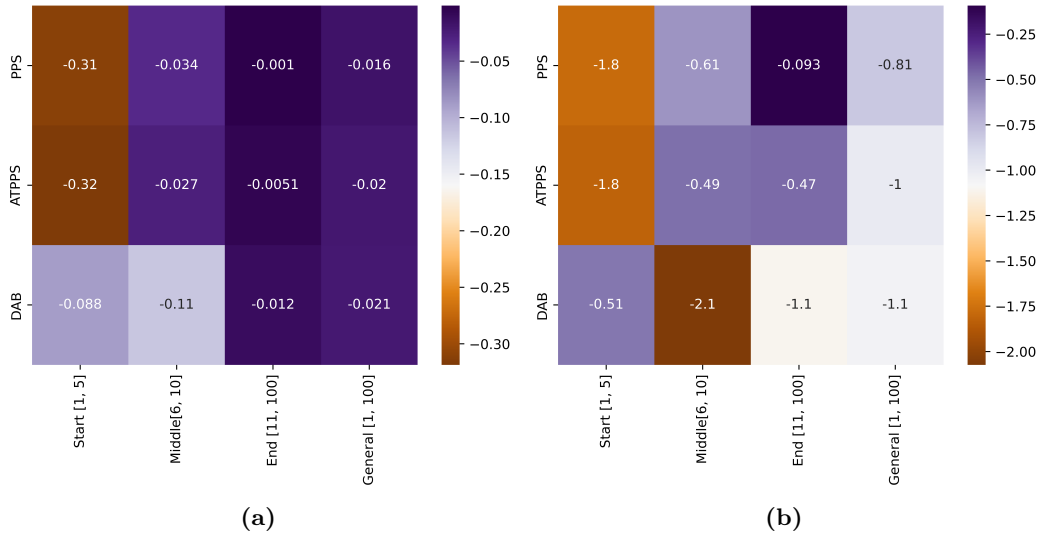

Figure 54: (32×32)-Ring of Cliques: heat map of slopes per region - log-linear and log-log

6.6.2 128x8 Ring of Cliques

The clique size plays a crucial role for the efficacy of the DAB algorithm. The decreased clique size favors the DAB, which reduces the error in the network more rapidly than the Push-Pull Sum based algorithms, as seen in figure 55. All the load balancing algorithms show a rapid decrease of error in the network, indicated by the steep negative slopes as visualized in figure 59 b). The Push-Pull Sum-based algorithms show an initial slope of -1.3, whereas the DAB achieves an even steeper -1.4 slope in the start region (rounds 1 to 5). After this initial sharp decline, the error reduction slows down. However, DAB still maintains the steepest slope, with an average reduction of -0.95 per round, followed by ATPPS (-0.89) and PPS (-0.79). The curves in this region are relatively flat, as observed in the log-log representation in figure 55 a). The decrease effect diminishes as the error of the network is already relatively low in the end region. At round 100, the final MSE values highlight the effectiveness of each algorithm. DAB achieves the lowest MSE of 10.64; ATPPS follows closely with 13.68. PPS results in the highest MSE of 22.33. Compared to the (32×32)-Ring of Cliques, the load balancing algorithms further reduced the error by 2 to 4 units. The ATPPS showed the most improvement, lowering the MSE by 5 units, followed by DAB (4 units) and PPS (2 units).

All three load balancing algorithms were fitted to fourth-degree polynomials. The best-fit equations are as follows: DAB's MSE data is fitted to a fourth-degree polynomial:

$$MSE_r = 5.45 \times 10^{-7} r^4 - 1.7 \times 10^{-4} r^3 + 0.02 r^2 - 1.33 r + 46.71 \tag{44}$$

(figure 56), as are the PPS:

$$MSE_r = 1.04 \times 10^{-6} r^4 - 3.41 \times 10^{-4} r^3 + 0.04 r^2 - 2.73 r + 97.58 \tag{45}$$

(figure 57) and the ATPPS:

$$MSE_r = 9.54 \times 10^{-7} r^4 - 2.93 \times 10^{-4} r^3 + 0.03 r^2 - 2.05 r + 67.02 \tag{46}$$

(figure 58).

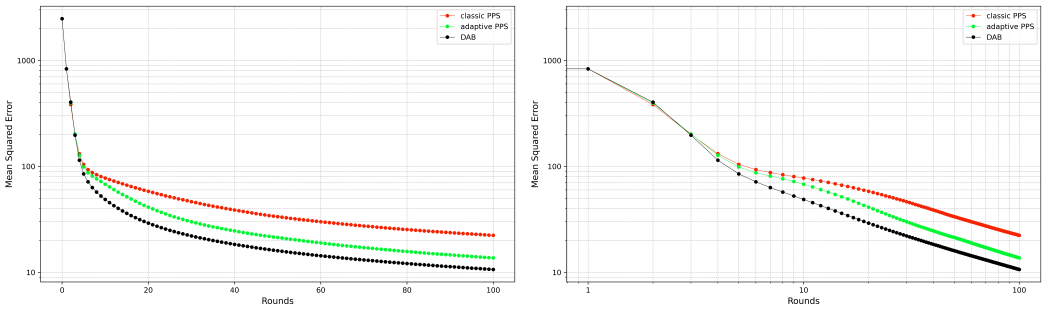

(a) **(b)**

Figure 55: (128 × 8)-Ring of Cliques: mean squared error per rounds (log-linear and log-log)

6.6.3 8x128 Ring of Cliques

Increasing the clique size and reducing the number of cliques favors the Push-Pull Sum-based algorithms (PPS and ATPPS), which exhibit a steep decrease in error during the first 5 rounds of the simulation (figure 60). PPS and ATPPS achieve an error reduction of approximately -2 on average for the start region. DAB shows a more moderate decrease of -0.12 in the same period. The error reduction slows as the network reaches a balanced state, since the error of the network is already very low, and the network is in a state of good balance, showing an MSE in this region of around -30 for the Push-Pull Sum-based algorithms. In the middle region, the state of the network managed by the DAB is still very unbalanced, thus the balance potential is higher. The Push-Pull Sum-based algorithms reduce the error by around -0.13 for the ATPPS and -0.01 for the PPS in the final region, while the DAB shows a still very high value of approximately -2.1. The steep decrease and the low

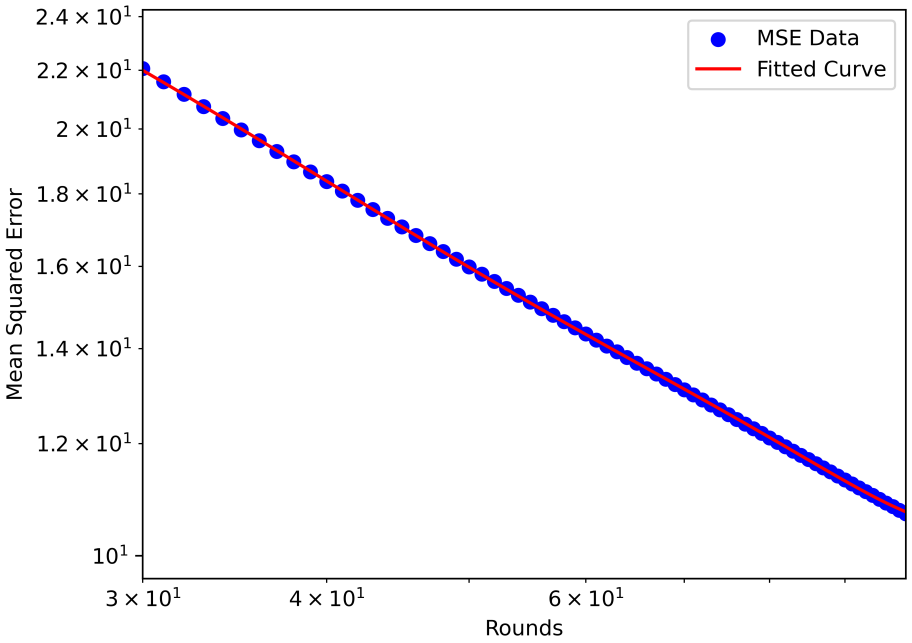

Figure 56: (128×8)-Ring of Cliques - polynomial regression fit: DAB

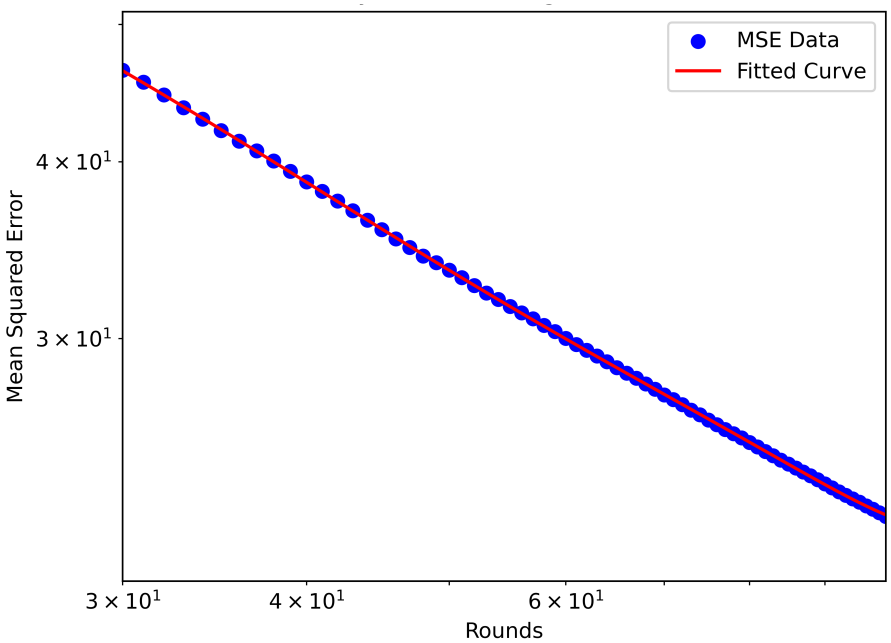

Figure 57: (128×8)-Ring of Cliques - polynomial regression fit: PPS

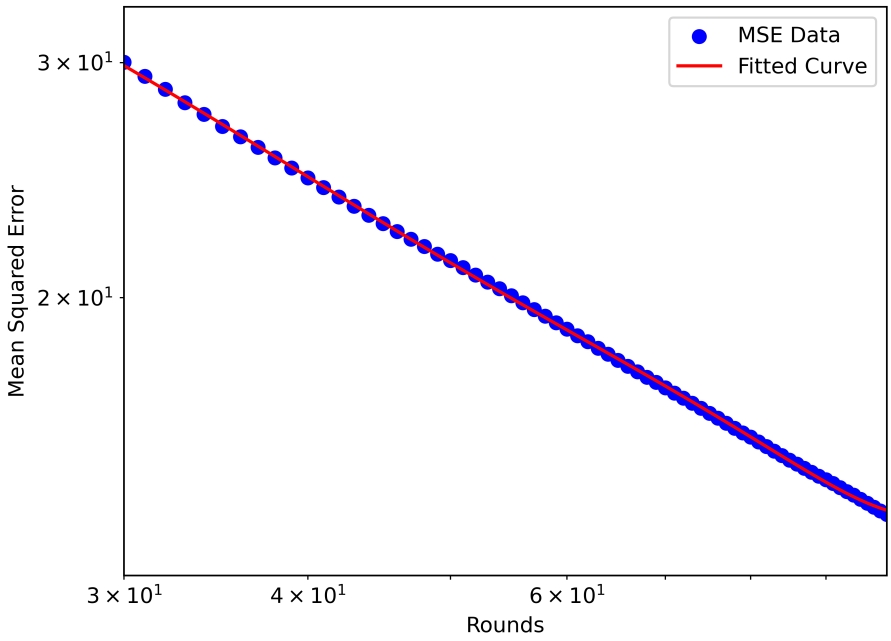

Figure 58: (128 × 8)-Ring of Cliques - polynomial regression fit: ATPPS

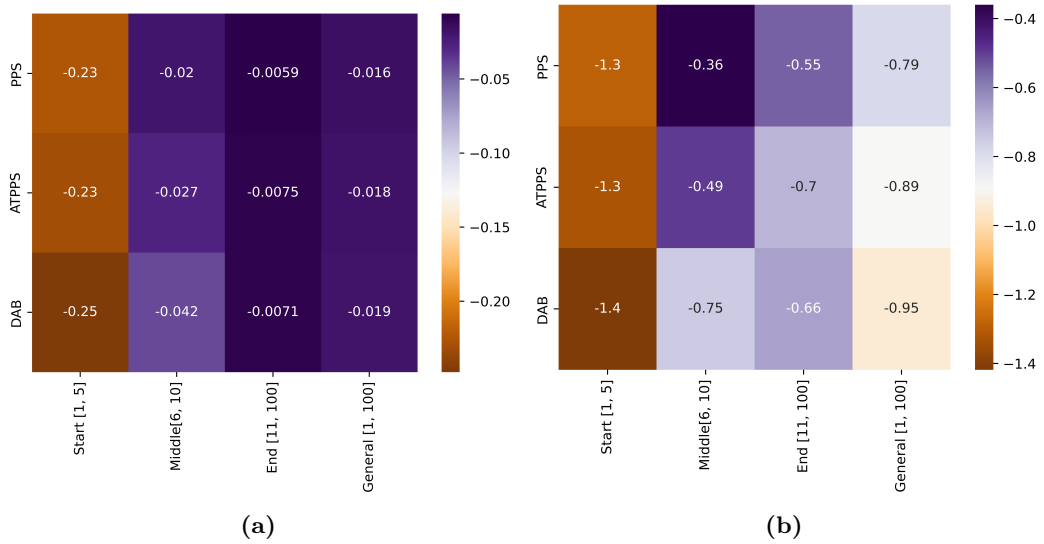

(a) **(b)**

Figure 59: (128 × 8)-Ring of Cliques: heat map of slopes per region - log-linear and log-log

MSE values after rounds 5 and 10 stem from the fast error reduction in the cliques. Compared to the experiment in the (8 × 128)-Ring of Cliques in 6.6.2, the error

after 100 rounds drops to lower values. The final MSE values for the DAB are 5.18 compared to 5.95 for the PPS and 4.56 for the ATPPS. Especially in the last region (rounds 12 to 100), the DAB catches up to the Push-Pull Sum-based algorithms. However, the PPS and ATPPS achieved a broadly balanced state of the network after round 10, dropping the error to an MSE value of 7. In the following rounds, the inter-clique error reduction follows. Here the PPS algorithm has difficulties, since the algorithm orders the nodes of the network to choose their transfer partner at random. The ATPPS has an advantage compared to the PPS here since it prioritizes the bridging nodes once its neighbors within the clique are already balanced. This elaborates why the PPS curve is mostly stagnating, while the ATPPS curve shows a downward trend. The stagnating trend between rounds 20 to 100 is expressed by the linear mode fit in figure 62. The best-fit model follows the equation

$$MSE_r = -1.5 * 10^{-3} r + 6.05. \tag{47}$$

The slope of $-1.5 * 10^{-3}$ is very small. The behavior of the PPS is captured by this simple model. It does not involve any accelerations like in the exponential model. The PPS curve shows a more complex relation between the MSE reduction over the rounds, namely a polynomial of degree 2 following the equation.

$$MSE_r = 6.07 \times 10^{-5} r^2 - 0.02r + 6.39 \tag{48}$$

(figure 62). The DAB does not follow a single power relationship in this region. Between rounds 15 and 50, the error reduction can be expressed by a third-degree polynomial

$$MSE_r = -3.33 \times 10^{-3} r^3 + 0.63r^2 - 40.23r + 872.75 \tag{49}$$

(figure 63 a)), while in later rounds the power relation is a bit more complex, expressed by a fourth-degree polynomial following the equation

$$MSE_r = 2.96 \times 10^{-6} r^4 - 9.97 \times 10^{-3} r^3 + 0.13 r^2 - 7.16 r + 161.73 \qquad (50)$$

(figure 63 b)).

Snippets of the simulation results confirm that within each clique, loads are balanced. However, inter-clique load balancing remains pending, which indicates that global equilibrium is not fully achieved. Listing 6.1 shows the simulation outcomes of two connected cliques balanced by the ATPPS in round 100. While the first clique converged to a value of around 46.35, the second clique averaged to approximately 47.90. The ground truth of the first clique is 45.89, and the ground truth of the second clique is 48.13. So the simulation outcomes and the ground truths align; however, the averages do not align with the ground truth of the Ring of Cliques (which is 49.09) itself. The PPS simulation outcomes show a similar behavior.

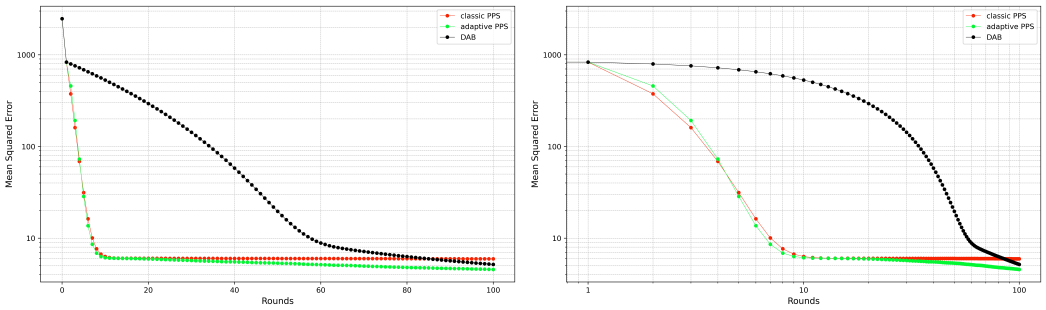

(a) **(b)**

Figure 60: (8×128)-Ring of Cliques: mean squared error per rounds (log-linear and log-log)

```
# First Clique starts here
ID 0      sum 23.703116631927735   weight 0.5112902995975737
Average 46.359410007551446
ID 1      sum 39.52476483621201    weight 0.852801600538612
```

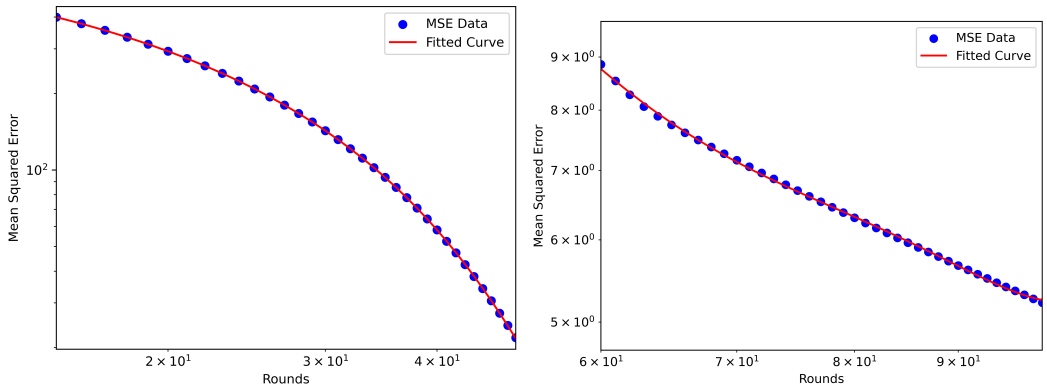

Figure 61: (8×128)-Ring of Cliques - polynomial regression fit: rounds 20-50 and 55-100

```
Average 46.34696371494727
ID 2     sum 8.793798989811481    weight 0.18958634077240344
Average 46.38413798158778
...
ID 125   sum 94.3005473042508     weight 2.0354736681273184
Average 46.32855181615266
ID 126   sum 145.10578299145917   weight 3.1321941681390815
Average 46.32719914604474
ID 127   sum 149.43516229432458   weight 3.222997634840688
Average 46.365272092950555
# First Cliques ends here

# Second Clique starts here
ID 128   sum 198.97437468622982   weight 4.149869252421544
Average 47.947143050380134
ID 129   sum 168.24642313171216   weight 3.5107838866374186
Average 47.92275131832632
ID 130   sum 35.6266112221637     weight 0.7449330697151406
```

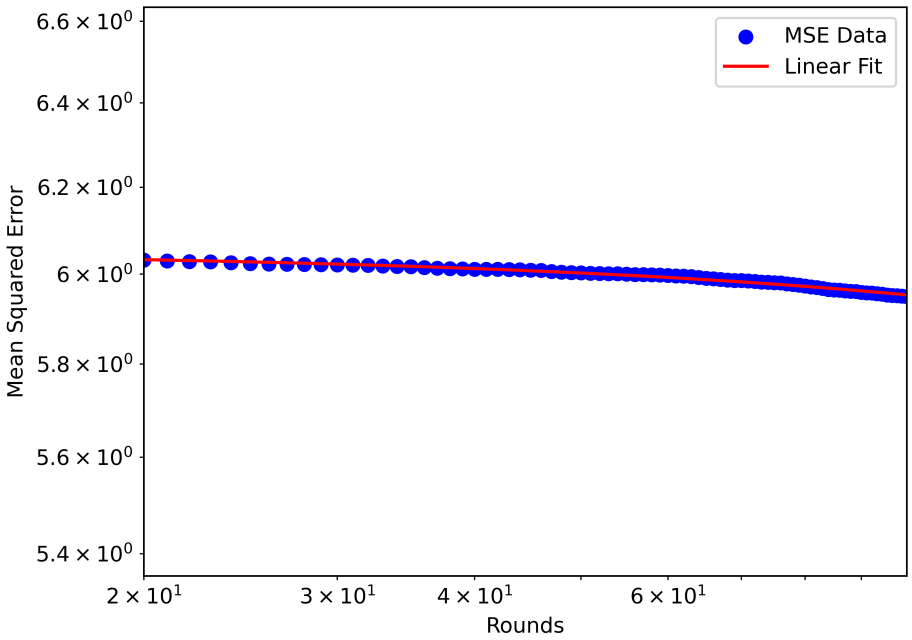

Figure 62: (8 × 128)-Ring of Cliques - linear regression fit: PPS

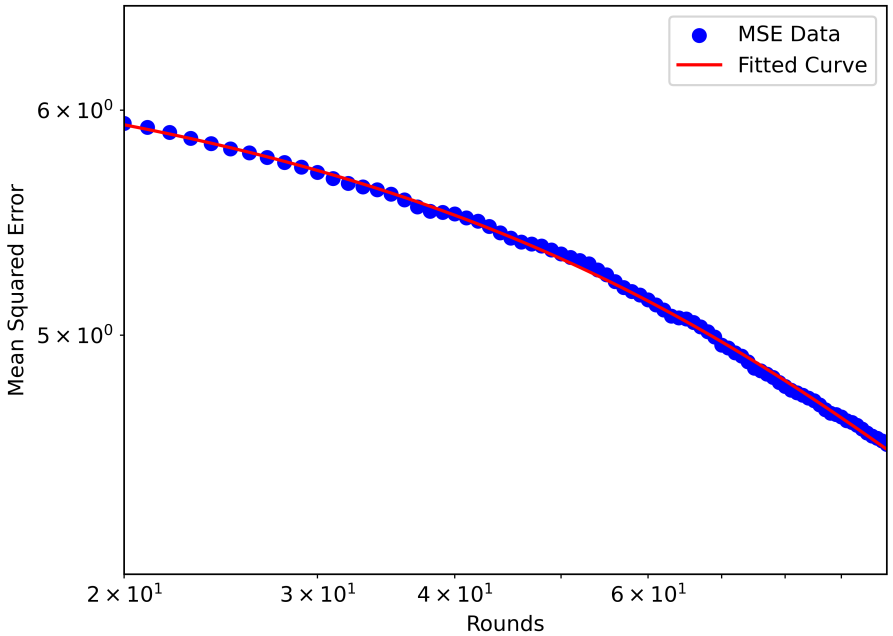

Figure 63: (8 × 128)-Ring of Cliques - polynomial regression fit: ATPPS

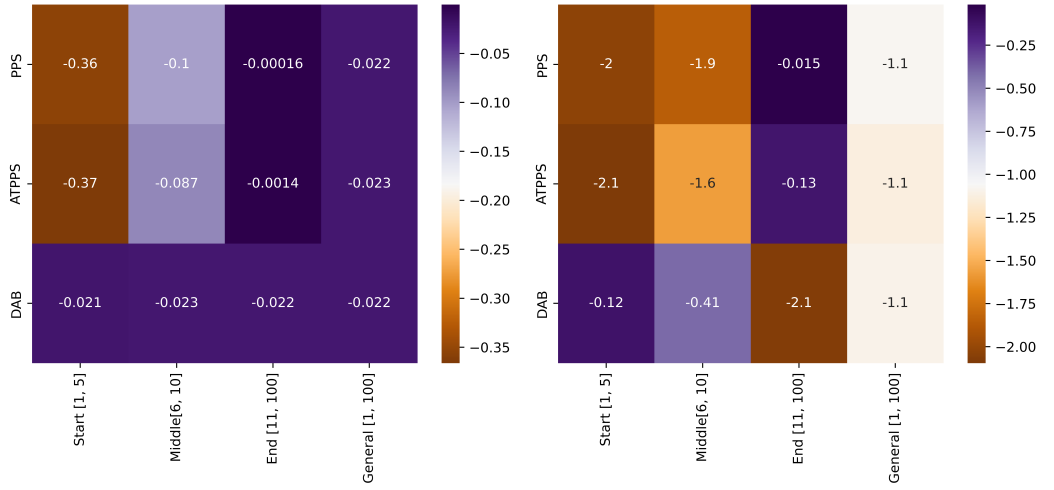

(a) **(b)**

Figure 64: (8×128)-Ring of Cliques: heat map of slopes per region - log-linear and log-log

```
Average 47.82525124812511
...
ID 253    sum 63.87360335784297    weight 1.3317373880292274
Average 47.962611797185005
ID 254    sum 15.173810743452982    weight 0.31637895519911763
Average 47.96087253623784
ID 255    sum 19.982619800226413    weight 0.4175626540105257
Average 47.85538076334456
# Second Cliques ends here
```

Listing 6.1: Snippet of simulation outcomes ATPPS: Experiment 2

7 Conclusion

The Adaptive Threshold Push-Pull Sum algorithm proves to be a compromise solution between the Push-Pull Sum and Single-Proposal Deal-Agreement-Based algorithms. The simulation results show that the Adaptive Threshold Push-Pull Sum algorithm performs well in dense graphs as well as in regular low-degree graphs. Especially for the Ring of Cliques $ROC_{32,32}$ and $ROC_{8,128}$ as well as for Lollipop $L_{512,512}$ and $L_{896,128}$ topologies, the ATPPS algorithm proved to be the best solution, as the algorithm achieved the lowest MSE values after 100 rounds of simulation. The Adaptive Threshold Push-Pull Sum achieved good overall results. In cases where the PPS failed to show good balancing abilities, like in the $ROC_{32,32}$, the Adaptive Threshold Push-Pull Sum proved to be very efficient, achieving results close to the Deal-Agreement-Based algorithm. In cases where the Push-Pull Sum algorithm achieved lower MSE within 100 rounds, the difference to the Adaptive Threshold Push-Pull Sum algorithm was not significant as seen for the Complete graph K_{1024}, Star graph S_{1024}, Lollipop graph $L_{128,896}$, as well as the Torus Grid $T_{32,32}$. However, when the Adaptive Threshold Push-Pull Sum outperforms the traditional Push-Pull Sum algorithm, the MSE discrepancies are more significant, like in the case of Ring of Cliques $ROC_{32,32}$ and $ROC_{128,8}$. The Adaptive Threshold Push-Pull Sum algorithm manages to distribute loads efficiently by adaptively adapting to the network state; this was particularly evident in the $ROC_{32,32}$ and $ROC_{128,8}$ structures. When the load differences within the cliques were no longer significant enough, clique-to-clique communication via the bridging nodes was favored. The Adaptive Threshold Push-Pull Sum algorithm also achieves the sharpest downward trend for K_{1024} until the

curve finally stagnates. No improvement of the load balancing behavior was observed for the Ring R_{1024} structure; the reason for this is that each node has exactly 2 neighbors, and thus the condition $\log_2(|neighbourhood|) =$ evaluates exactly one and thus acts very similar to the traditional Push-Pull Sum algorithm, without prioritizing any nodes. Also for the Star topology, the Adaptive Threshold does not achieve any advantage over the traditional Push-Pull Sum algorithm, as the leaf nodes all communicate with the central node; however, the condition with significant load transfers limits the number of requests to the central node compared to the traditional Push-Pull Sum algorithm. The result: the Push-Pull Sum achieves a balanced state of the network earlier. Compared to the Push-Pull Sum algorithms, the Single-Proposal Deal-Agreement-Based algorithm has problems with dense graphs, such as the Complete graph, Lollipop graph with a large clique size, and Ring of Cliques with a large clique size. The MSE differences in the 100th round are extremely large because the MSE differences for low-degree topologies such as the Ring graph and the Torus Grid graph are not as significant. The Adaptive Threshold Push-Pull Sum is localized by the MSE between the other two algorithms, closer to the best-performing Deal-Agreement-Based algorithm than to the traditional Push-Pull Sum algorithm. The simulation results depend mainly on the sensibility factor k. A large k ensures a more sensitive selection of neighbors, while a smaller k allows a coarser selection of neighbors.

8 Acknowledgments

First and foremost, I would like to thank...

- advisers
- examiner
- person1 for the dataset
- person2 for the great suggestion
- proofreaders

9 Appendix

9.1 Model Fitting

The model fitting was carried out with *SciPy* and *NumPy* in the python programming language. In the case of the exponential model fit *SciPy* provides a optimizer *scipy.optimizer*, which provides the **curve_fit** method [17]. This method uses the Levenberg-Marquardt method to solve non-linear least squared problems. *NumPy* delivers the **polyfit** method, which was used to fit the MSE data to the polynomial model described in equation 13. The linear regression is achieved using *scipy.stats* **linregress** method, which calculates a linear least-squares regression for two sets of data points for x and y [18].

9.1.1 Levenberg-Marquardt Method

The Levenberg-Marquardt method is a hybrid of the Gauss-Newton method and the Levenberg-method (Trust-Region approach). Starting from an initial guess for the parameters, the Levenberg-Marquardt method uses the Jacobian matrix to estimate how changes in parameters affect the fitted function. Then a damped least squared step is applied, where if the parameters are far from optimal, the Levenberg-Marquardt method behaves like the gradient descent, and if the parameters are near optimal the Levenberg-Marquardt method acts like the Gauss-Newton method. It

minimizes the sum of the squared residuals:

$$f(x) = \frac{1}{2}\sum_{j=1}^{m} r_j^2(x) = \frac{1}{2}||r||^2, \tag{51}$$

where $f(x)$ is the objective function that we are trying to minimize, $r_j(x)$ represent the residuals (which are the differences between the observed data and the model predictions), $r(x)$ is the vector of residuals, where $r(x) = [r_1(x), r_2(x), ..., r_n(x)]^T$. $||r||^2$ is the squared Euclidean norm of the residual vector, which sums the squared differences. The Gauss-Newton method is modified by a damping coefficient λ and is written as:

$$(J^T J + \lambda I)p = J^T r(x), \tag{52}$$

where J is the Jacobian matrix of $r(x)$ (the derivatives of the residuals), I is the identity matrix and λ controls the step size (a large λ leads to gradient descent, small λ lead to the Gauss-Newton method). $J^T J$ is the approximation of the Hessian matrix. p is the update step. This equation is solved iteratively reducing $f(x)$ until the parameters converge.

If λ is large, the equation behaves like the gradient descent:

$$\lambda I p = J^T r(x), \tag{53}$$

while a small λ causes the equation to behave like the Gauss-Newton method:

$$J^T J p = J^T r(x). \tag{54}$$

[19] [20] [21]

9.1.2 Linear Regression by SciPy

SciPy's **linregress** method fits data to a simple linear model as depicted in equation 12. It achieves this by solving the *Ordinary Least Squares* regression which minimizes the sum of squared residuals. It returns the slope and the intercept of the fitted line, as well as the *R-value* (*Pearson's R*), *p-value*, standard error of the estimated slope and the standard error of the estimated intercept. [18] [22]

9.1.3 polyfit and polyval by Numpy

The *numpy.polyfit* method fits a polynomial of a given degree to a set of data points using the least squares minimization method [23]. This method constructs the Vandermonde Matrix of a degree d and a set of data points $(x_1, y_1), (x_2, y_2), ..., (x_n, y_n)$ of form:

$$V = \begin{bmatrix} x_1^d & x_1^{d-1} & \dots & x_1^1 & 1 \\ x_2^d & x_2^{d-1} & \dots & x_2^1 & 1 \\ \vdots & \vdots & \ddots & \vdots & \vdots \\ x_n^d & x_n^{d-1} & \dots & x_n^1 & 1 \end{bmatrix} \tag{55}$$

Each row represents one data point, and each column corresponds to a power of x. Following the construction of the Vandermonde-matrix, the polynomial coefficients $c = [c_d, c_{d-1}, ..., c_0]$ are computed by solving:

$$c = (V^T V)^{-1} V^T y. \tag{56}$$

This method solves the linear least squares and ensures that the sum of squared residuals is minimized:

$$\sum_{i=1} (y_i - P(x_i))^{2^n}, \tag{57}$$

where $P(x_i)$ is the polynomial function. [23] [24] [25]

Once the polynomial coefficients are computed, the polynomial is evaluated using numpy's **polyval** method. This method internally uses the *Horner's method* in order to reduce the number of multiplications. For the polynomial of form:

$$P(x) = a_n x^n + a_{n-1} x^{n-1} + \cdots + a_1 x + a_0 \tag{58}$$

this method outputs a polynomial of form:

$$P(x) = p_0 x^n + p_1^{n-1} + \cdots + p_n. \tag{59}$$

[26]

9.2 Overview of Simulation Outcomes

The simulation outcomes are presented in the tables 2, 3, 4, 5, 6, 7 8, 9, 10 and 11. The tables contain the equations for the fitted models, the slopes in all regions and the MSE value after 100 rounds of execution of the algorithms.

Table 2: Simulation Overview - Complete graph: Fitted Model, Slopes per Region, and Final MSE

Topology		**Fitted Model**	**Slope (log-linear)** Rounds 1–10	Rounds 11–65	Rounds 66–100	Rounds 1–100	MSE_{100}
K_{1024}	DAB	**Rounds 1–100:** $MSE_r = 844.63 \cdot e^{-0.01r}$	-2.6×10^{-3}	-2.7×10^{-3}	-3.0×10^{-3}	-2.8×10^{-3}	436.85
	PPS	**Rounds 10–80:** $MSE_r = 2530.41 \cdot e^{-0.9r}$	-0.38	-0.39	-0.16	-0.31	1.73×10^{-28}
	ATPPS	**Rounds 10–65:** $MSE_r = 4309.94 \cdot e^{-1.06r}$	-0.43	-0.46	-0.02	-8.4	5.63×10^{-28}

Table 3: Simulation overview - Star graph: fitted model, slopes per region, and final MSE

Topology		**Fitted Model**	**Slope (log-linear)** Rounds 1–10	Rounds 11–45	Rounds 46–100	Rounds 1–100	MSE_{100}
S_{1024}	DAB	**Rounds 1–100:** $MSE_r = 840.42 \cdot e^{-0.01r}$	-2.3×10^{-3}	-2.3×10^{-3}	-2.5×10^{-3}	-2.4×10^{-3}	480.48
	PPS	**Rounds 10–45:** $MSE_r = 29794.60 \cdot e^{-1.39r}$	-0.5	-0.6	-4.8×10^{-3}	-0.26	8.31×10^{-25}
	ATPPS	**Rounds 18–60:** $MSE_r = 9329.40 \cdot e^{-1.05r}$	-0.45	-0.45	-0.11	-0.26	6.52×10^{-24}

Table 4: Simulation overview - Ring graph: fitted model, slopes per region, and final MSE

Topology		**Fitted Model**	**Slope (log-log)** Rounds 1–10	Rounds 11–69	Rounds 70–100	Rounds 1–100	MSE_{100}
R_{1024}	DAB	**Rounds 10–60:** $MSE_r = 1.72 \times 10^{-5} r^4 - 2.30 \times 10^{-3} r^3 + 0.19 r^2 - 5.99 r + 114.83$	-1.1	-0.51	-0.5	-0.78	22.41
	PPS	**Rounds 10–60:** $MSE_r = 2.99 \times 10^{-5} r^4 - 0.5 \times 10^{-2} r^3 + 0.32 r^2 - 9.68 r + 166.30$	-0.93	-0.55	-0.52	-0.74	27.68
	ATPPS	**Rounds 10–60:** $MSE_r = 3.04 \times 10^{-5} r^4 - 0.5 \times 10^{-2} r^3 + 0.32 r^2 - 9.64 r + 161.86$	-0.95	-0.56	-0.49	-0.75	26.56

Table 5: Simulation overview - Torus Grid: fitted model, slopes per region, and final MSE

Topology		**Fitted Model**	**Slope** Rounds 1–10	Rounds 10–39	Rounds 40–100	Rounds 1–100	MSE_{100}
$T_{32,32}$	DAB	**Rounds 10–39:** $MSE_r = -1.35 \times 10^{-6} r^5 + 1.89 \times 10^{-4} r^4 - 0.01 r^3 + 0.30 r^2 - 4.6 r + 34.10$ **Rounds 40–100:** $MSE_r = -6.01 \times 10^{-6} r^3 + 1.66 \times 10^{-3} r^2 - 0.16 r + 6$	-2.1	-1.2	-2	-1.7	436.85
	PPS	**Rounds 10–39:** $MSE_r = -3.65 \times 10^{-6} r^5 + 5.16 \times 10^{-4} r^4 - 0.03 r^3 + 0.83 r^2 - 12.52 r + 88.16$ **Rounds 40–100:** $MSE_r = -1.15 \times 10^{-5} r^3 + 3.205 \times 10^{-3} r^2 - 0.33 r + 13.72$	-1.5	-1.2	-1.4	-1.4	1.73×10^{-28}
	ATPPS	**Rounds 10–39:** $MSE_r = -5.54 \times 10^{-6} r^5 + 7.65 \times 10^{-4} r^4 - 0.04 r^3 + 1.16 r^2 - 16.81 r + 112.86$ **Rounds 40–100:** $MSE_r = -9.99 \times 10^{-6} r^3 + 2.8034 \times 10^{-3} r^2 - 0.28 r + 11.29$	-1.6	-1.3	-1.7	-1.5	5.63×10^{-28}

Table 6: Simulation overview - $L_{512,512}$: fitted model, slopes per region, and final MSE

Topology		**Fitted Model**	**Slope (log-log)** Rounds 1–7	Rounds 8–50	Rounds 51–100	Rounds 1–100	MSE_{100}
$L_{512,512}$	DAB	$MSE_r = -5.89 \times 10^{-5} r^3 + 0.03 r^2 - 5.68 r + 459.42$	-0.34	-0.32	-1.1	-0.44	108.90
	PPS	$MSE_r = 8.44 \times 10^{-7} r^4 - 2.52 \times 10^{-4} r^3 - 0.03 r^2 - 1.64 r + 56.68$	-1.3	-0.56	-0.51	-0.88	14.71
	ATPPS	$MSE_r = 8.69 \times 10^{-7} r^4 - 2.56 \times 10^{-4} r^3 + 0.03 r^2 - 1.62 r + 54.48$	-1.3	-0.57	-0.51	-0.89	13.82

Table 7: Simulation overview - $L_{128,896}$: fitted model, slopes per region, and final MSE

Topology		**Fitted Model**	**Slope (log-log)** Rounds 1–7	Rounds 8–50	Rounds 51–100	Rounds 1–100	MSE_{100}
$L_{128,896}$	DAB	$MSE_r = 3.46 \times 10^{-6} r^4 - 1.12 \times 10^{-3} r^3 + 0.14 r^2 - 7.69 r + 190.78$	-0.86	-0.87	-0.78	-0.84	17.47
	PPS	$MSE_r = -3.72 \times 10^{-8} r^5 + 1.31 \times 10^{-5} r^4 - 1.85 \times 10^{-3} r^3 + 0.13 r^2 - 4.96 r + 84.91$	-1.2	-1.3	-1.1	-1.2	3.31
	ATPPS	$MSE_r = 1.59 \times 10^{-6} r^4 - 4.74 \times 10^{-4} r^3 + 0.054 r^2 - 2.94 r + 70.59$	-1.2	-1.1	-1.5	-1.2	3.41

Table 8: Simulation overview - $L_{896,128}$: fitted model, slopes per region, and final MSE

Topology		**Fitted Model**	**Slope (log-log)** Rounds 1–7	Rounds 8–50	Rounds 51–100	Rounds 1–100	MSE_{100}
$L_{896,128}$	DAB	$MSE_r = -1.93 \times 10^{-4} r^3 + 0.05 r^2 - 5.33 r + 745.95$	-0.08	-0.1	-0.11	-0.09	542.09
	PPS	$MSE_r = 2.00 \times 10^{-7} r^4 - 6.01 \times 10^{-5} r^3 + 6.95 \times 10^{-3} r^2 - 0.39 r + 13.44$	-2	-0.59	-0.47	-1.2	3.59
	ATPPS	$MSE_r = 2.28 \times 10^{-7} r^4 - 6.77 \times 10^{-5} r^3 + 7.68 \times 10^{-3} r^2 - 0.42 r + 13.62$	-2	-0.61	-0.5	-1.2	3.27

Table 9: Simulation overview - $ROC_{32,32}$: fitted model, slopes per region, and final MSE

Topology		**Fitted Model**	**Slope (log-log)** Rounds 1–5	Rounds 6–10	Rounds 11–100	Rounds 1–100	MSE_{100}
$ROC_{32,32}$	DAB	$MSE_r = -5.89 \times 10^{-5} r^3 + 0.03 r^2 - 5.68 r + 459.42$	-0.51	-2.1	-1.1	-1.1	6.55
	PPS	$MSE_r = 8.44 \times 10^{-7} r^4 - 2.52 \times 10^{-4} r^3 - 0.03 r^2 - 1.64 r + 56.68$	-1.8	-0.61	-0.09	-0.81	19.80
	ATPPS	$MSE_r = 8.69 \times 10^{-7} r^4 - 2.56 \times 10^{-4} r^3 + 0.03 r^2 - 1.62 r + 54.48$	-1.8	-0.49	-0.47	-1	8.42

Table 10: Simulation overview for $ROC_{128,8}$: fitted model, slopes per region, and final MSE

Topology		**Fitted Model**	**Slope (log-log)** Rounds 1–5	Rounds 6–11	Rounds 12–100	Rounds 1–100	MSE_{100}
$ROC_{128,8}$	DAB	$MSE_r = 5.45 \times 10^{-7} r^4 - 1.7 \times 10^{-4} r^3 + 0.02 r^2 - 1.33 r + 46.71$	-1.4	-0.75	-0.66	-0.95	10.64
	PPS	$MSE_r = 1.04 \times 10^{-6} r^4 - 3.41 \times 10^{-4} r^3 + 0.04 r^2 - 2.73 r + 97.58$	-1.3	-0.36	-0.55	-0.79	22.33
	ATPPS	$MSE_r = 9.54 \times 10^{-7} r^4 - 2.93 \times 10^{-4} r^3 + 0.03 r^2 - 2.05 r + 67.02$	-1.3	-0.49	-0.7	-0.89	13.68

Table 11: Simulation overview - $ROC_{8,128}$: fitted model, slopes per region, and final MSE

Topology		**Fitted Model**	**Slope (log-log)** Rounds 1–5	Rounds 6–11	Rounds 12–100	Rounds 1–100	MSE_{100}
$ROC_{8,128}$	DAB	$MSE_r = -3.33 \times 10^{-3} r^3 + 0.63 r^2$ $-40.23r + 872.75$ **Rounds 60-100:** $MSE_r = 2.96 \times 10^{-6} r^4 - 9.97 \times 10^{-3} r^3$ $+0.13 r^2 - 7.16r + 161.73$	-0.12	-0.41	-2.1	-1.1	5.18
	PPS	$MSE_r = 6.07 \times 10^{-5} r^2 - 0.02r + 6.39$	-2	-1.9	-0.01	-1.1	5.95
	ATPPS	$MSE_r = -0.0015x + 6.05$	-2.1	-1.6	-0.13	-1.1	4.56

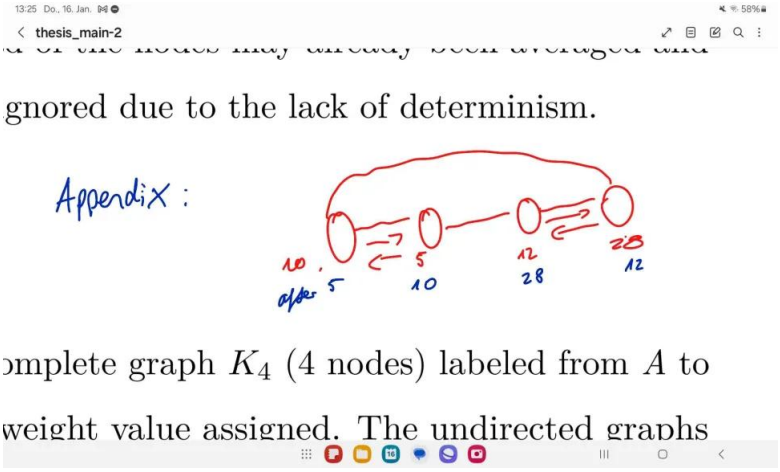

Figure 65: Example Ring Graph

ToDo Counters

To Dos: 0;

Parts to extend: 0;

Draft parts: 0;

Bibliography

[1] S. Nugroho, A. Weinmann, and C. Schindelhauer, *Adding Pull to Push Sum for Approximate Data Aggregation.* Springer, 2023.

[2] D. Kempe, A. Dobra, and J. Gehrke, "Gossip-based computation of aggregate information," in *44th Annual IEEE Symposium on Foundations of Computer Science, 2003. Proceedings.*, pp. 482–491, 2003.

[3] Y. Dinitz, S. Dolev, and M. Kumar, "Local deal-agreement algorithms for load balancing in dynamic general graphs," *Theory of Computing Systems*, vol. 67, pp. 348–382, Apr 2023.

[4] C. Xu and F. C. Lau, *Load Balancing in Parallel Computers: Theory and Practice.* USA: Kluwer Academic Publishers, 1997.

[5] C. Schindelhauer, "Lecture notes in graph theory," 2021.

[6] E. Bayazitoglu, "Comparative analysis of load balancing algorithms in general graphs." University of Freiburg, 2024.

[7] M. A. Iqbal, J. H. Saltz, and S. H. Bokhari, "A comparative analysis of static and dynamic load balancing strategies," in *International Conference on Parallel Processing, ICPP'86, University Park, PA, USA, August 1986*, pp. 1040–1047, IEEE Computer Society Press, 1986.

[8] S. Banerjee and D. Sarkar, "Hypercube connected rings: A scalable and fault-tolerant logical topology for optical networks," *Computer Communications*, vol. 24, pp. 5–6, 2001.

[9] P. Mahlmann, *Peer-to-peer networks based on random graphs.* PhD thesis, University of Paderborn, 2010. Paderborn, Univ., Diss., 2010.

[10] V. P. Vidomenko, "The traffic self-guidance for multimedia communications," *Automation of the Russian Academy of Sciences*, 1997. Accessed on January 11, 2025.

[11] D. B. West, *Introduction to Graph Theory.* Pearson; Pearson Education, Inc., 2nd, reprint ed., 2002. Includes solution manual.

[12] A. O. Jayeola and P. T. Ayomide, "Modelling and assessment of the star network topology using opnet simulation techniques," *International Journal of Scientific Research in Computer Science and Engineering*, vol. 11, no. 1, pp. 14–22, 2023.

[13] J. Jonasson, "Lollipop graphs are extremal for commute times," *Random Structures & Algorithms*, vol. 16, no. 2, pp. 131–142, 2000.

[14] Drakos, N. and Moore, R., *PeerSim: HOWTO: Build a new protocol for the PeerSim 1.0 simulator*, December 2005. Accessed: August 13, 2024.

[15] J. Lorenzo, "Graphing by hand and on computer," 2000. Accessed: 2025-02-10.

[16] H. Motulsky and A. Christopoulos, *Fitting Models to Biological Data Using Linear and Nonlinear Regression: A practical guide to curve fitting.* 10 2023.

[17] S. Community, *SciPy curvefit Documentation*, 2024. Accessed: 2025-02-12.

[18] S. Community, *SciPy linregress Documentation*, 2024. Accessed: 2025-02-12.

[19] H. P. Gavin, "The levenberg-marquardt algorithm for nonlinear least squares curve-fitting problems," 2020. Accessed: 2025-02-11.

[20] J. J. Moré, "The levenberg-marquardt algorithm: Implementation and theory," in *Numerical Analysis* (G. A. Watson, ed.), (Berlin, Heidelberg), pp. 105–116, Springer Berlin Heidelberg, 1978.

[21] T. Brox, "Lecture notes in optimisation, lecture 3: Newton- and quasi-newton methods," 2014-2020.

[22] A. Wooditch, N. J. Johnson, R. Solymosi, J. Medina Ariza, and S. Langton, *Ordinary Least Squares Regression*, pp. 245–268. Springer International Publishing, 2021.

[23] N. Community, *NumPy polyfit Documentation*, 2024. Accessed: 2025-02-12.

[24] Y. Li and X. Ding, "Vandermonde determinant and its applications," *Journal of Education and Culture Studies*, vol. 7, p. p16, 10 2023.

[25] G. I. of Technology, *Least Squares Approximation*, 2024. Accessed: 2025-02-12.

[26] W. D. Project, "Horner's method," 2024. Accessed: 2024-02-08.